Vicinage effect for hydrogen clusters in Si_3N_4 and SiO_2

A. L'Hoir,[1] C. Cohen,[1] J. J. Ganem,[1,*] I. Trimaille,[1] I. C. Vickridge,[1] and S. M. Shubeita[2]
[1]*INSP, SAFIR, Université Pierre et Marie Curie and CNRS, 75005 Paris-cedex, France*
[2]*Instituto de Física da Universidade Federal do Rio Grande do Sul, Avenida Bento Gonçalves 9500, 91501-970 Porto Alegre, Rio Grande do Sul, Brazil*

(Received 7 December 2011; revised manuscript received 19 March 2012; published 27 April 2012)

We have measured the evolution with depth z of the vicinage effect and Coulomb explosion for H_2^+ and H_3^+ molecular ions traversing thick, uniform amorphous targets of Si_3N_4 and SiO_2. High depth resolution is achieved by scanning the energy per nucleus of the incoming molecules E_b around the energy E_R corresponding to narrow resonances in the cross sections of $^{18}O(p,\alpha)^{15}N$ at 151 keV and in $^{15}N(p,\alpha\gamma)^{12}C$ at 429 keV. The corresponding reaction yield $Y(E_b)$ is, to first order, inversely proportional to the stopping force $S_{\rm mol}$ on the molecular fragments, giving a direct image of the evolution of the vicinage effect and Coulomb explosion with z. At the target surface, the vicinage effect enhances the stopping force on the molecules by a factor $\chi > 1$. As they penetrate the matter, the distance between the molecule nuclei increases, as a consequence of Coulomb explosion and multiple scattering lateral displacement, and the vicinage effect decreases with depth z. The experiment yields information on the screened Coulomb repulsive potential via the repulsion velocity $V^{\rm lim}$ observed at large z, where the distances R_{ij} between the molecule nuclei are large compared to the adiabatic cutoff $R_{\rm ad}$ (no vicinage effect). We show that the first order view, that $Y(Eb) \propto S_{\rm mol}^{-1}$, is profoundly modified by the energy fluctuations induced by the Coulomb explosion and lateral multiple scattering. Our observations are satisfactorily reproduced when modeled using a dynamic screening radius r_s in the range $R_{\rm ad}$ (for H_3^+) to $2R_{\rm ad}$ (for H_2^+) for the Coulomb explosion and the evolution with R_{ij} of χ given by the dielectric model for the interaction of the exploding molecules with the target electron gas.

DOI: 10.1103/PhysRevA.85.042901 PACS number(s): 34.50.Bw, 79.77.+g

I. INTRODUCTION

When a high-velocity molecular ion (n atoms) travels in a dense medium, the stopping force on each ion of the molecule is partially due to the polarization of the medium induced by the neighboring ions of the molecule. The stopping force $S_{\rm mol}$ on the molecule is hence different from the value $S_{\rm add}$ given by a simple additivity rule ($\chi = S_{\rm mol}/S_{\rm add} \neq 1$). This phenomenon is the vicinage effect, which has been studied both experimentally [1–5] and theoretically [6–11] over several decades. Depending on the ion velocity $V_{\rm ion}$, the distance R_{ij} between the nuclei ($i = 1,n$, $j = i + 1,n$), the orientation of the molecule, and the medium, χ may be larger or smaller than 1.

As they penetrate into matter, the nuclei composing the molecule are progressively separated, a consequence of both screened Coulomb repulsion ("Coulomb explosion") and lateral displacement induced by multiple scattering (MS) on each nucleus of the molecular ions. Multiple scattering is by far dominated by elastic collisions of these nuclei on target nuclei screened by their own electrons. Thus, the distance R_{ij} between the nuclei of the molecule, initially equal to R_0, increases with traveled depth z. When R_{ij} exceeds the adiabatic cutoff $R_{\rm ad} = V_{\rm ion}/\omega_p$ (where $V_{\rm ion}$ is the translation velocity of the molecule in the target frame and ω_p is a plasmon frequency associated with the loosely bound target electrons), typically $R_{ij} \gtrsim 2R_{\rm ad}$, each ion travels as an independent particle; that is, $\chi \simeq 1$. On the contrary, a strong vicinage effect ($\chi \neq 1$) is observable for small R_{ij}, typically for $R_{ij} \lesssim R_{\rm ad}$.

From a theoretical point of view it is of great interest to follow the molecular breakup dynamics and vicinage effect experimentally from the state corresponding to the initial molecule to that of fully independent nuclei. In a recent short communication [12], we showed that this is possible with high depth resolution by recording yield curves in the vicinity of narrow resonances of nuclear reactions. In practice, molecular beams are sent onto thick layers of uniform composition (traversed path length $z_{\rm max}$) formed on an inert substrate. The beam nuclei may induce on one of the layer elements a nuclear reaction with a cross section presenting a narrow resonance (resonance energy E_R). One then measures the nuclear reaction yield $Y(E_b)$ as a function of the beam energy E_b per nucleon when the energy per incoming nucleus is close to E_R (see Sec. II). The path length $z_{\rm max}$ is chosen such that the nuclei reaching the layer-substrate interface can be considered as fully separated. One may then obtain, in principle, two major pieces of information. (i) The shape of the yield curve corresponding to nuclear reactions induced at the layer-substrate interface depends on the limit velocity $V^{\rm lim}$ of the nuclei of the exploding molecules in the projectile center-of-mass (c.m.) frame, which can then be determined, giving access to the screened Coulomb repulsive potential governing the explosion of the molecules. The kinematics of this explosion: Evolution with time $R_{ij}(t)$ of the distance between the nuclei of the molecule, or evolution with depth $R_{ij}(z)$, can then be deduced. (ii) To first order (see Sec. II C), for $E_b > E_R$, nuclear reactions occur at given depth $z(E_b)$, where the internuclear distance is $R_{ij}[z(E_b)]$. Moreover, $Y(E_b)$ is inversely proportional to the stopping force $S_{\rm mol}$ on the molecule. Hence, the $Y(E_b)$ yield curve give access to the evolution with R_{ij} of the stopping force on molecules, $S_{\rm mol}(R_{ij})$.

*jean-jacques.ganem@insp.jussieu.fr

In fact, as is shown in this paper, the experimental data analysis is much more complicated than suggested from the above first-order approach. Energy fluctuations, in particular those induced by the Coulomb explosion velocities when projected on the beam direction, play a major role here: There is no one-to-one correspondence between z, R_{ij}, and $S_{\rm mol}$. One of the major aims of this paper is to overcome this difficulty (see Fig. 14 and more generally Sec. III) in order to reliably extract valuable information from our experimental data.

In order to study the Coulomb explosion at various ion velocities and the evolution of the stopping power with the distance between the molecule nuclei in media with different dielectric responses, we have performed two sets of experiments, with H_2^+ and H_3^+ molecules (H^+ beams were also used as a reference).

(a) H_n^+ molecules ($n = 1,2,3$), produced by the high energy resolution Van de Graaff accelerator of the Institut des NanoSciences de Paris, were sent into amorphous thick ^{18}O-enriched SiO_2. We then used the narrow resonance of the $^{18}O(p,\alpha)^{15}N$ nuclear reaction at 151 keV/A, measuring the α yield $Y_\alpha(E_b)$. In this experiment, $R_{\rm ad} = 2.8$ a.u. is larger than the initial mean distance R_0 between the molecule nuclei, and the stopping force is enhanced ($\chi > 1$). A preliminary analysis of the experimental results was presented in Ref. [12].

(b) The same molecules as in (a) were sent into amorphous thick ^{15}N-enriched Si_3N_4. We used the $^{15}N(p,\alpha\gamma)^{12}C$ narrow resonance at 429 keV and measured the γ yield $Y_\gamma(E_b)$. $V_{\rm ion}$ is higher by a factor 1.68 than in (a) and perturbative approaches are then more justified here. Since the ω_p are rather close for SiO_2 and Si_3N_4, (see below), $R_{\rm ad}$ is higher in experiment (b) and the vicinage effect persists for larger R_{ij} distances. Moreover, the influence of MS is decreased for increasing velocities. The γ yield is much higher than Y_α measured in (a) (larger cross section), leading to much better statistics. Hence, the experiment in Si_3N_4 is a more severe test of the vicinage effect coupled to Coulomb explosion than that in SiO_2. As we shall see, when analyzing the Si_3N_4 experimental results, paradoxical features show up that are also present in the SiO_2 experiment but, owing to the statistics, were not detected in Ref. [12].

Unless otherwise mentioned, in what follows atomic units are used. When necessary, we use $n = 1,2,3$ to index the parameters associated, respectively, with H^+, H_2^+, and H_3^+.

II. EXPERIMENT

A. Si_3N_4

A ^{15}N-enriched Si_3N_4 target was obtained by plasma-enhanced chemical-vapor deposition on a Si (001) crystal, using SiH_4 (silane) and a 99% enriched nitrogen gas $^{15}N_2$. The stoichiometry of the layer was determined by nuclear reaction analysis (NRA); we found $Si_3N_{3.8}H_{1.4}$, close to the expected Si_3N_4. The influence of this departure from the Si_3N_4 stoichiometry on our results and their analysis is negligible, since the mean valence electron density is very close to that of Si_3N_4, within 1%. Moreover, we expect no hydrogen desorption for the beam fluences used in our experiments (Si_3N_4 is used as a hydrogen storage layer), and thus no additional desorption-induced energy-loss fluctuations may be feared.

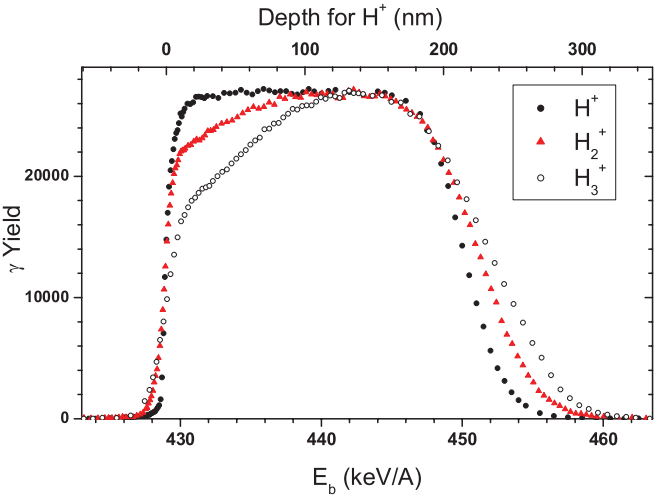

FIG. 1. (Color online) Measured γ yields when scanning the beam energy E_b for H_n^+ ions in Si_3N_4 ($E_R = 429$ keV/A). The samples are tilted at 68° (mean path length $z_{\rm max} \simeq 220$ nm). An indicative depth scale z is also given.

The total measured amount of ^{15}N is $n_{15} = 4.31 \times 10^{17}$ cm^{-2} (thickness $\simeq$82 nm, assuming a density $\rho = 3.1$ g/cm^3). In the reaction chamber, the nitride sample was mounted on a sample holder that allows x-y translation and a rotation (tilt). The pressure in the chamber was below 10^{-7} mbar. The beam current varies from $\approx$1.5 μA for H_2^+ beams to $\approx$0.3 μA for H_3^+. The γ rays from the $^{15}N(p,\alpha\gamma)^{12}C$ nuclear reaction were detected by a BGO ($Bi_4Ge_3O_{12}$) detector located just behind the sample holder, outside the vacuum chamber.

The beam energy E_b was scanned from below the resonance energy $E_R = 429$ keV/A to above E_R using an automatic scanning system [13]. For a given beam energy, one measures the total accumulated γ yield $Y(E_b)$ in the BGO for a given beam fluence. In Fig. 1, the yield curves $Y(E_b)$ obtained with H^+, H_2^+, and H_3^+ ion beams are compared. A very large solid angle Ω was used in order to improve statistics, with no consequence on the shape of the $Y(E_b)$ curves, since the γ emission is nearly isotropic. The beam fluences for a given E_b were, respectively, 10, 5, and 3.33 μC for H^+, H_2^+, and H_3^+, according to the number of fragments resulting from the molecular breakup of the molecules. The sample was tilted to $\simeq$68° in order to increase the apparent sample thickness.

In order to minimize the beam-induced damage, the yield curves for each ion were recorded on different impact points (diameter 1.5 mm). The total dose on each point was about 1000 μC. A second sweeping of the beam energy on the same points has shown that the influence of carbon buildup and beam damage have negligible influence on the shape of the $Y(E_b)$ curves.

B. SiO_2

The experimental results obtained for 151 keV/A H^+, H_2^+, and H_3^+ in SiO_2 were given in Ref. [12]. We reproduce the α yield curve $Y_\alpha(E_b)$ in Fig. 2.

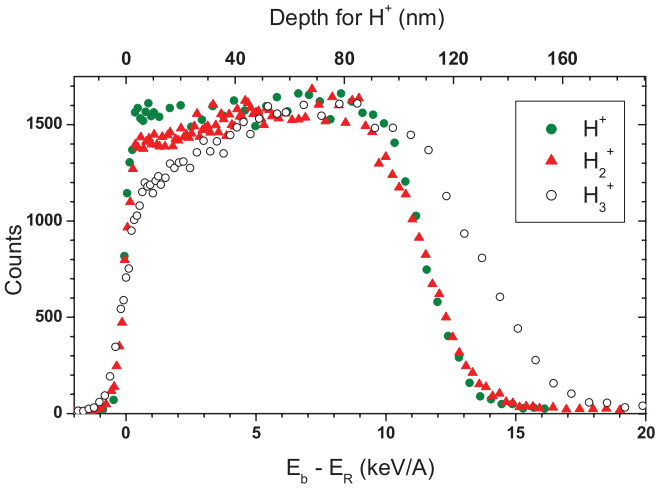

FIG. 2. (Color online) Measured α yields when scanning the beam energy E_b for H_n^+ ions in SiO_2 ($E_R = 151$ keV/A). Oxide thickness 54 nm for H^+ and H_2^+ and 60 nm for H_3^+. Samples were tilted at 60° (corresponding mean path lengths $z_{max} \simeq 108$ and 120 nm). α particles are detected using a 300 mm^2 silicon surface barrier detector (solid angle ≈2 sr). An indicative depth scale z is also given.

The $Y_\alpha(E_b)$ were obtained with 5 times larger beam fluences than for Si_3N_4, but, owing to the much lower cross section, they result in much poorer statistics.

Note that the traversed path lengths z_{max} were different for the different ions (see caption of Fig. 2).

C. Qualitative analysis, first-order approach

The discussion is based on the Si_3N_4 experiment (better statistics, very close z_{max} values for the three beams) but could be applied to the SiO_2 experiment as well. We first consider the proton beam (see Fig. 1). When $E_b < E_R$, the resonance is never reached and $Y(E_b) \approx 0$. For $E_b > E_R$, when traveling in the target the beam loses energy and reaches E_R around a depth $z(E_b)$ where the resonant nuclear reaction can take place. $Y(E_b)$ is then proportional to the ^{15}N concentration $C(z)$ around $z(E_b)$. As we increase E_b, $z(E_b)$ eventually reaches the interface between the nitride and the silicon substrate and the yield begins to decrease, falling to ≈0 for higher beam energies. Since $C(z)$ is constant throughout the nitride layer, one observes essentially a constant plateau. The shape of the leading edge of $Y(E_b)$ around $E_b = 429$ keV is a consequence of the incident beam energy fluctuations and of the resonance width Γ_R. The shape of the falling edge (around $E_b = 450$ keV), is governed by the energy loss straggling of the beam, dominated by violent collisions on target electrons.

As shown in Ref. [12], $Y(E_b)$ is related to the stopping force and to the resonance width Γ_R. Briefly, neglecting all causes of fluctuations, $Y(E_b)$ corresponds to nuclear reactions around depth $z(E_b)$, in a slice of matter with thickness δz such that the beam energy is in the range $\approx[E_R - \Gamma_R/2, E_R + \Gamma_R/2]$; that is, $\Gamma_R \approx S(E_R)\delta z$, where $S(E_R)$ is the stopping power at the energy of the resonance. $Y(E_b)$, which is proportional to δz, is then proportional to $1/S(E_R)$, whatever E_b, if one neglects any fluctuations, leading to the observed constant plateau.

The H^+ $Y(E_b)$ curve yields a mean energy loss of 21.2 keV for the proton beam throughout the tilted layer. The density ρ of amorphous nitride is 3.1 g/cm^{-3} which gives, using the stopping powers given by the code CASP [14], a total path length $z_{max} = 218$ nm. Assuming a 99% enriched layer, from the measured n_{15} and stoichiometry, the nitride thickness should be 85.9 nm, leading to $z_{max} = 229$ nm, assuming a 68° tilt angle. This thickness is 5.0% higher than the value 218 nm based on the CASP S_p value. This disagreement may originate from uncertainties on the tilt angle (a perfect agreement is obtained for an angle of 66.8°), on the value n_{15} measured, on the measured stoichiometry, on the isotopic enrichment assumed, and on the measured energy loss, but also on the CASP prediction itself. To simplify, in what follows we assume the CASP stopping power to be valid for isolated protons.

We now consider the $Y(E_b)$ curves obtained with very high statistics for the two molecular ions. Due to possible vicinage effect, the stopping force per nucleus on the molecule, $S_{vic}(E_R) = S_{mol}(E_R)/n$, may be different from the stopping force $S_p(E_R) = 98.4$ eV/nm on an isolated proton (CASP value). At least five features show up in Fig. 1.

(i) A large decrease of $Y(E_b)$ in the energy range $E_R \lesssim E_b \lesssim E_R + 10$ keV, a signature of a vicinage effect, about twice larger for H_3^+ than for H_2^+. Since to first order $Y(E_b)$ is proportional to $1/S_{vic}(E_R)$, one has $S_{vic}(E_R) > S_p(E_R)$ ($\chi > 1$). For larger E_b, the vicinage effect disappears and the plateau yield $Y(E_b)$ reaches that for H^+: Due to Coulomb repulsion and MS, the distance R_{ij} between the molecule nuclei is much larger than R_{ad} and the nuclei behave as independent particles. To first order, the yield evolution with E_b gives a direct vision of the Coulomb explosion and of the evolution of the vicinage effect with the distance R_{ij} between the nuclei. To guide the eye, a depth scale based on the CASP $S_p(E_R)$ is displayed on the top of Fig. 1 (the corresponding depth scales for the molecules are somewhat shorter and nonlinear). When compared to Fig. 2 for the same molecules at 151 keV/A in silicon oxide, one can notice that the depth λ^{vic} over which a vicinage effect is observable at 429 keV/A is about twice that observed at 151 keV/A. The main reason for this is a larger adiabatic cutoff at high velocity. We also observe that close to the layer entrance, the vicinage effect seems larger in the nitride than in the oxide.

(ii) The magnitude of the falling slope at high energy ($E_b \approx 450$ keV) decreases from H^+ to H_3^+. This is a signature of the Coulomb explosion. In this region of the yield curve, the distance R_{ij} between the nuclei of molecules is large and in the projectile c.m. frame, the nuclei get a velocity V^{lim}, which depends on the initial distance R_0 and on the screening of the repulsive potential. In the laboratory frame and for an isotropic population of molecules, this gives rise to large energy fluctuations, proportional to V^{lim} at the layer-substrate interface [see Sec. III F and Eq. (7)], which add up independently with the collisional energy fluctuations (those for H^+). The energy fluctuations induced by the explosion are much higher for H_3^+ than for H_2^+ since a nucleus is repelled by two neighboring nuclei for the former against only one for the latter.

(iii) The beam energy values E_b^{int} required to reach the interface with the silicon substrate at energy E_R, increase from H^+ to H_3^+. This is also a signature of the vicinage effect: Over a large fraction of the layer thickness, one has $S_{vic}(E_b) > S_p(E_b)$ and the vicinage effect is larger for H_3^+ than for H_2^+. For

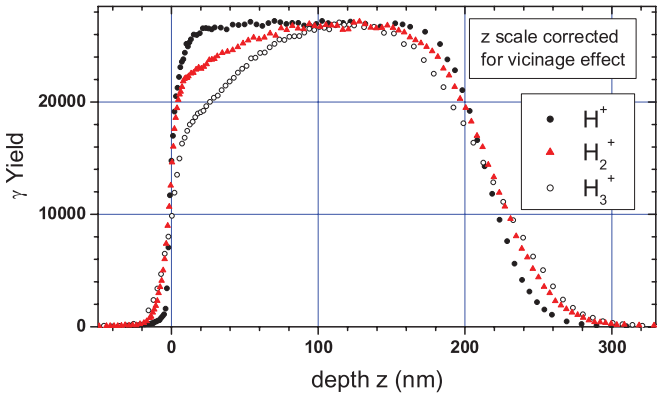

FIG. 3. (Color online) Measured γ yields ($E_R = 429$ keV/A) as a function of depth z for H_n^+ ions in Si_3N_4 (see text for depth scale estimation).

Si_3N_4, one finds respectively $E_b^{\rm int} - E_R = 21.2$, 22.3, and 22.9 keV for H^+, H_2^+, and H_3^+, respectively. This is a measure of the cumulative effect of vicinage throughout the nitride. However, in order to avoid beam-induced damage, the impact points are different for the three ions and a small relative variation of the layer thickness would give rise to very large uncertainties when comparing the above $E_b^{\rm int} - E_R$ rather close values (for the SiO_2 experiment, the tilt angle was not kept constant and $E_b^{\rm int} - E_R$ bears no really significant information).

(iv) The rising slope around $E_b = E_R$ decreases from H^+ to H_3^+. For H^+, this slope depends on the resonance width and the beam energy resolution. For molecular ions, the vibration of the atoms in the incident molecules increases the energy fluctuations for each nucleus. A larger increase is observed for H_3^+ than for H_2^+. A careful analysis of the rising slope for H^+ using the code SPACES [15–17] (see Sec. II D) shows that there is some exchange between ^{15}N and ^{14}N close to the nitride surface.

(v) One observes in Fig. 1 that the vicinage effect disappears at larger depth for H_3^+ than for H_2^+, when using the depth scale only strictly valid for H^+. This depth scale may be corrected to first order by taking into account the experimental yield $Y(E_b)$ and using the $S_{\rm vic} \propto 1/Y(E_b)$ approximate law. This led to the yields $Y(z)$ of Fig. 3 for Si_3N_4.

With this more realistic z scale, the vicinage effects now disappears within the statistical errors, for similar depths for the two ions, $\lambda_2^{\rm vic} \simeq \lambda_3^{\rm vic} \simeq 90$ nm. This is a very surprising result since the repulsive force should be much larger for the triatomic molecule than for the diatomic one, leading to a shorter lifetime ($\lambda_3^{\rm vic}$ value) for vicinage. Indeed, as discussed in (ii), the comparison of the falling slopes clearly demonstrates that the repulsive potential was stronger for H_3^+. There is then a strong contradiction, and we are led to conclude that the shapes of the experimental curves for molecular ions, before reaching the plateau corresponding to H^+ ions, do not directly reflect the evolution with penetration depth of $S_{\rm vic}$, as assumed in (i). In fact, neglecting the energy fluctuations induced by the explosion (and also MS) is a very crude approximation. In what follows, we indicate how we have been able to account for these fluctuations and then to extract from our experiments a reliable and accurate description of the evolution of the vicinage effect with penetration depth. For this purpose, a code was written to simulate the yield curves. The physics underlying the code is fully detailed in Sec. III.

D. Quantitative analysis of the H^+ yield curve

The yield curve $Y_1(E_b)$ for H^+ may be considered as a standard corresponding to no vicinage effect and should then be carefully analyzed first. Here we only consider the case of Si_3N_4. The shape of $Y_1(E_b)$ depends on

(i) the beam energy dispersion, assumed to be Gaussian, with standard deviation σ_b;

(ii) the resonance shape, which is a Lorentzian with full width at half maximum (FWHM) $\Gamma_R = 120$ eV [18,19].

It also depends on

(iii) the possible presence of a thin contamination layer;

(iv) the shape of the concentration curve $C(z)$ for ^{15}N.

In principle, $C(z)$ should equal $C_{\rm bulk}$ throughout the sample. However, some exchange between the ^{15}N nuclei in the layer and the ^{14}N nuclei in the atmosphere may take place in the very surface region. If any, we assume a concentration variation given by the complementary error function Erfc:

$$C(z) = C_{\rm bulk} - (C_{\rm bulk} - C_s){\rm Erfc}(z/z_{\rm ech}), \qquad (1)$$

where $z_{\rm ech}$ is a characteristic depth and C_s the surface ^{15}N concentration.

Finally, the shape of $Y_1(E_b)$ depends on

(v) the energy-loss fluctuations of the proton beam.

For small thicknesses the energy spread is not Gaussian. In order to calculate $Y_1(E_b)$ with high precision, we used the code SPACES, which calculates the energy-loss distribution through sums of autoconvolutions [15,17]. The best overall fit of the experimental $Y_1(E_b)$ curve for protons in Si_3N_4 is presented in Fig. 4. It corresponds to $C_s/C_{\rm bulk} = \alpha_s = 0.78$ and $z_{\rm ech} = 9.7$ nm. We have also included a contamination layer (hydrocarbons, with zero ^{15}N concentration), equivalent to a 1.2-nm-thick nitride layer. For our high energy resolution Van de Graaff accelerator, the best fit corresponds to $\sigma_b = 106$ eV [250 eV FWHM]. At large depths, corresponding to the total traversed path ($z_{\rm max} \simeq 216$ nm), the proton energy-loss spectrum calculated in SPACES is nearly Gaussian with variance

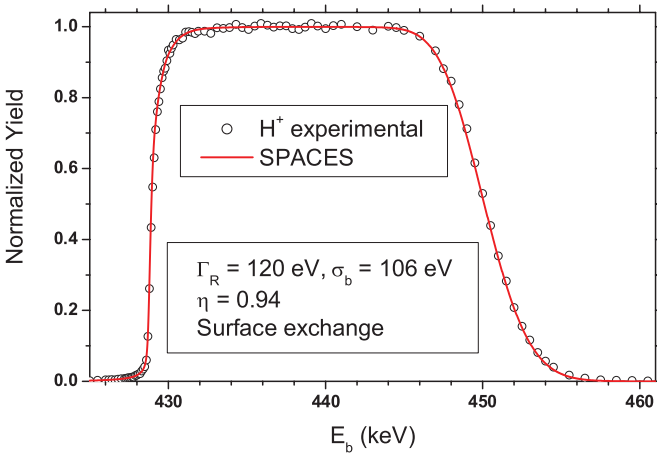

FIG. 4. (Color online) Fitting the γ yield curve $Y_1(E_b)$ for protons in Si_3N_4, using the code SPACES (total path length $z_{\rm max} = 116$ nm).

Ω^2_{expt}. We have compared Ω^2_{expt} to the Bohr [20] free target electron approximation Ω^2_B [Eq. (2)]:

$$\Omega^2_B \simeq 4\pi n_{\text{tot}} z, \tag{2}$$

where n_{tot} is the total target electron density (including core electrons, that is, 70 electrons per Si_3N_4 molecule), by introducing the ratio $\eta = \Omega^2_{\text{expt}}/\Omega^2_B$ which should be very close to 1 at large proton velocities. In Fig. 4, the best fit of the high-energy descending slope of $Y(E_b)$ is obtained for $\eta = 0.94$, a very reasonable value for 429-keV protons in a medium with mean atomic number $Z_2 = 70/7 = 10$. The corresponding value for 151-keV protons in SiO_2 [12] is $\eta = 0.80$.

For all further calculations corresponding to molecular ions, we keep the same α_s, z_{ech}, and Γ_R values and contamination layer as for protons. For $z_{\max}$ we allow for small variations (that do not exceed 3%) since the beam impacts are at different positions, and σ_b is replaced by $\sigma_{bv} > \sigma_b$ as the energy fluctuations associated to thermal vibrations in the incident molecules also contribute to the slope of the leading edge (the index bv stands for "beam and vibration").

III. FITTING THE RESULTS OBTAINED WITH MOLECULAR BEAMS: CALCULATION CODE AND ASSOCIATED PHYSICS

A. The molecules, thermal vibrations

The molecules, which are produced in the RF ion source, occupy excited vibrational states. For these homonuclear molecules, dipole radiation transition is ruled out and molecules enter the target in the excited states in which they are produced, influencing not only the relative velocities of the nuclei, but also their mean separation $\langle R_{ij}\rangle$. For H_2^+ the $R_{12} = R_0$ distribution was measured for a similar ion source [21], with a most probable value $R_m = 1.17$ Å, instead of 1.08 Å in the ground state. The distribution is broad and asymmetrical with an estimated mean value $\langle R_0\rangle \approx 1.48$ Å larger than the value $\langle R_o\rangle = 1.29$ Å used in Ref. [8], estimated from the Franck-Condon principle [22], and a FWHM $L_{12} \approx 0.8$ Å. The H_3^+ molecules are equilaterally triangular in shape [23] with $\langle R_{ij}\rangle = \langle R_0\rangle = 0.88$ Å in the ground state [24] and $\langle R_0\rangle$ in the range 0.95 Å to ≈1.2 Å when experimentally measured [23] in three different laboratories. A distribution of $\langle R_0\rangle$ was also measured in Ref. [23] and found to be very broad and asymmetrical (tail toward high R_0), with a FWHM very close to its mean value. As we see below, the R_0 distributions (mainly their mean value and to a lesser extent, their width), play an important role on the shape of the yield curves measured in our experiments. These distributions should hence be known with some precision if one wants to extract from the yield curves reliable information on the vicinage effect and on the Coulomb explosion of the molecules. However, the R_0 distributions most probably depend on the particular conditions in which the molecular ions were produced in the ion source. For instance, as shown later, our measurements indicate that, both for H_2^+ and for H_3^+, the initial velocity distributions associated with the vibrating nuclei in the c.m. frame were smaller in the experiments performed at 151 keV/A than in those performed at 429 keV/A. We do not have a direct experimental access to the R_0 distributions. Thus, we have attempted to take benefit both of the distributions found in the literature and of our measurements providing the initial velocity distributions of the nuclei in the molecule (c.m. frame) in order to determine a realistic range for the $\langle R_0\rangle$ values and for the widths of the R_0 distributions corresponding to the molecules used in our experiments.

B. History of a molecule

When entering the layer, the distance R_{ij} between the nuclei and the vibrational velocity V_{th} varies from one molecule to another. The molecular ions dissociate close to the target entrance ($z = 0$). For 429 keV/A H_2^+ and H_3^+ in Si_3N_4, the cross section σ_D for dissociation is of the order of 1.5×10^{-16} cm^2 (taken from [25] for the same molecules in neon, which corresponds to the same atomic number $Z_2 = 10$ as the nitride mean atomic number); it corresponds to a mean free path $\Lambda_D = 0.7$ nm (using the density $\rho = 3.1$ for nitride, that is, an atomic concentration $N_A = 9.33 \times 10^{22}$ at. cm^{-3}). For the SiO_2 experiment, the cross sections are ≈2 times larger ($\Lambda_D = 0.35$ nm, extrapolated from [25]). The time scale for dissociation is orders of magnitude smaller than the period associated with molecular vibration. Thus, the position and velocity of the nuclei in a given molecule may be considered as frozen in their initial state before Coulomb explosion. R_{ij} and V_{th} are then random variables distributed around their mean values. There are at least two consequences for the shape of the yield curves $Y(E_b)$.

(i) Velocity fluctuations lead to energy fluctuations at the sample surface, influencing the slope of the leading edge.

(ii) To R_{ij} fluctuations correspond fluctuations in the initial potential energy just after dissociation of the molecule. This in turn implies fluctuations for the Coulomb repulsive velocities. The implication of these fluctuations is discussed in Appendix D. Following the dissociation, the distance R_{ij} between the nuclei in the molecule varies: It increases due to the repulsive interaction between the nuclei and also due to the elastic collisions on the target nuclei.

The perturbation of the target electron gas induced by the molecule depends on the orientation of the molecule with respect to the beam direction. Hence, even in an isotropic medium (silicon nitride, silicon oxide), the repulsive potential $V(\mathbf{R}_{ij})$ which depends on the dynamic perturbation of the target electron gas induced by the molecule, is not isotropic. The small-angle MS of the nuclei of the molecules on the target nuclei induces independent random lateral displacements of each molecule nucleus; that is, $\mathbf{R}_{ij}$ are random vectors. The mean distance $\langle R_{ij}\rangle$ increases with depth and the orientation of the molecule varies. Clearly, an exact description of the evolution with time of a molecule entering the crystal with a given orientation is an involved task. However, the molecules in the incident beam are randomly oriented, and we may assume that these orientations are isotropically distributed. The experimentally observed effects are then an average over these orientations, but one needs, in principle, to describe the detailed history of molecules for given initial orientations, including the MS, the anisotropy of the vicinage effect and that of $V(\mathbf{R}_{ij})$. Then and only then an average should be taken over the various orientations. Huge simplifications are brought about when averaging first over the orientations of

the molecule, that is, using an isotropically averaged vicinage effect and an isotropic repulsive potential $V(R_{ij})$. This is a strong assumption, extensively used in the literature and that we have adopted. It is mainly questionable for the fraction of the molecules entering the target with an internuclear axis close to the beam orientation. For these molecules, the contribution of the wake potential to $V(\mathbf{R}_{ij})$ does indeed induce a departure from the hypothesis of isotropy. Also, when averaging so early, at least one source of energy-loss fluctuations is omitted since the energy loss is orientation dependent when vicinage takes place (see Sec. III C and Appendix A).

C. Stopping power, vicinage effect, and molecule orientation

When averaged over isotropically oriented molecules, the contribution of the loosely bound target electrons to the stopping force on molecules (n nuclei) may be expressed as [11]

$$S_{\text{mol-val}} = \frac{2}{\pi V_{\text{ion}}^2}\int_0^\infty \frac{dq}{q}\int_0^{qV} d\omega\omega \text{Im}\left(\frac{-1}{\epsilon(q,\omega)}\right) \times\left[\sum_{i=1}^{n} Z_i^2 + 2\sum_{i>j} Z_i Z_j \frac{\sin(qR_{ij})}{qR_{ij}}\right], \quad (3)$$

where the R_{ij} are the internuclear distances and $\epsilon(q,\omega)$ is the generalized valence dielectric function; the imaginary part $\text{Im}[-1/\epsilon(q,\omega)]$ is the so-called energy-loss function (ELF); ω and q may be associated, respectively, with the energy and momentum transfers between the incident particles and the medium. One may also rewrite Eq. (3) as

$$S_{\text{mol-val}} = S_p\left(\sum_{i=1}^{n} Z_i^2\right) + 2\sum_{i>j} Z_i Z_j K_{ij}(R_{ij}),$$

where S_p stands for the stopping force on an isolated proton and the K_{ij} are interference terms describing the vicinage effect. At large R_{ij}, the K_{ij} vanish and the stopping force on the molecule is simply the sum of individual stopping forces on the atoms in the molecule. In the present experiment, all the Z_i are equal to 1.

In order to estimate the energy-loss fluctuations induced by anisotropy, we consider the simple case of H_2^+ molecules and of the so-called single-pole (SP) approximation. In this description of the dielectric response, damping is omitted and the ELF is given by

$$\text{Im}\left(\frac{-1}{\epsilon(q,\omega)}\right) = \frac{\pi\omega_p^2}{2\omega_q}\delta(\omega-\omega_q), \quad (4)$$

where $\omega_q^2 = \omega_p^2 + q^4/4$; this approximation is valid at high velocity ($V \gg v_F$, where v_F is the electron gas Fermi velocity). For a vector $\mathbf{R}_{12}$ joining the two nuclei, with projection $d = R_{12}\cos\theta$ on the beam direction and projection $\rho = R_{12}\sin\theta$ in the transverse plane, the stopping force on the molecule is given by (SP approximation)

$$S_{\text{mol-SP}}(R_{12},\theta) = \frac{4\pi n_e}{V_{\text{ion}}^2}\int_{q_1}^{q_2}\frac{dq}{q}\big[Z_1^2+Z_2^2 + 2Z_1Z_2J_o(q\rho)\cos(\omega_q d/V)\big], \quad (5)$$

TABLE I. Binding energies in atomic Si and N (the number of electrons in each subshell is indicated in brackets). Contribution S_{shell} of each shell to the H^+ stopping power of Si_3N_4 (in eV/nm, assuming a $\rho = 3.1$ g cm^{-3} density) for 429-keV protons, as calculated by CASP in the unitary convolution approximation [14] (multiply S_{shell} by 0.750 to convert into 10^{-15} eV cm^2/molecule units).

Shell	B_{Si} (eV)	B_{N} (eV)	S_{shell}
1*s*	1825.3 (2)	406 (2)	1.0
2*s*	152.1 (2)	24.1 (2)	20.0
2*p*	109.5 (6)	12.5 (3)	44.4
3*s*	14.5 (2)		15.0
3*p*	7.4 (2)		18.0
Total electrons	14	7	98.4

where J_o is the zero-order Bessel function of the first kind. At large molecule velocity, $q_1 \simeq \omega_p/V_{\text{ion}} = 1/R_{\text{ad}}$ and $q_2 \simeq 2V_{\text{ion}}$. When isotropically averaged, the oscillating factor $J_o(q\rho)\cos(\omega_q d/V)$ in Eq. (5), which governs the interference term K_{12}, reduces to $\sin(qR_{12})/qR_{12}$ [see Eq. (3)], and the integral calculation is analytical:

$$S_{\text{mol-SP}}(R_{12}) = \frac{4\pi n_e}{V_{\text{ion}}^2}\big\{\big(Z_1^2+Z_2^2\big)\ln\big(2V_{\text{ion}}^2/\omega_p\big) + 2Z_1Z_2 \times[F(u_1)-F(u_2)]\big\}, \quad (6)$$

where $u_1 = q_1R_{12}$, $u_2 = q_2R_{12}$, $F(u) = \sin u/u - C_i(u)$, and C_i is the cosine integral function.

We show in Appendix A that the anisotropy of the vicinage effect [Eq. (5)] induces energy-loss fluctuations that can be neglected to first order.

D. Valence electrons, H^+ stopping power, and energy-loss function

1. *Case of 429 keV/A molecular ions on Si_3N_4*

One may partition the electrons in the Si_3N_4 molecule into valence and core electrons. When considering binding energies B_{Si} and B_{N} in Table I, for electrons in the L shell of N and in the M shell of Si, the corresponding valence binding energies B_{val} are below or equal to 24.1 eV = 0.89 a.u. $\lesssim \omega_p$. These 32 electrons per molecule (4.57 electron/atom) may hence be considered as valence electrons. Assuming a density $\rho = 3.1$ g cm^{-3}, the corresponding plasma frequency ω_p of the uniform valence free electron gas is $(4\pi n_e)^{1/2} = 0.891$ a.u. (Fermi velocity $v_F = 1.37$ a.u., electron density $n_e = 0.0632$ a.u.). The remaining 38 electrons per molecule have binding energies B_{core} larger than 4 a.u. and may be considered as core electrons. Table I also gives the stopping power S_{shell} of silicon nitride for protons, calculated using the unitary convolution approximation (UCA) [14]. For $E_b = E_R$, the CASP total stopping $S_{\text{tot}} = 98.4$ eV/nm is very close to the stopping and range of ions in matter [26] semiempirical value, 95.6 eV/nm. One may hence estimate with precision the relative contribution of valence and core electrons to the stopping of 429-keV protons ($V_{\text{ion}} = 4.14$ a.u.): The contribution of valence electrons amounts 82% of the total stopping force $S_{\text{tot}} = 98.4$ eV/nm. According to Eq. (6), the high velocity approximation gives a H^+ valence stopping of 87 eV/nm, using the plasma frequency $\omega_p = 0.89$ a.u. of the

free electron model. This value, calculated in the high velocity approximation, is then only 8% higher than the more involved CASP result for 429-keV protons. In the present experiment, core electrons do not contribute to the vicinage effect: The corresponding adiabatic cutoff is $R_{\text{ad-core}} \lesssim V_{\text{ion}}/B_{\text{core}} = 1.0$ a.u., smaller than the initial distance R_0 between the nuclei in the molecule ($\simeq$2.4 and 1.8 a.u., respectively, for H_2^+ and H_3^+). Since the vicinage effect comes only from the valence electrons, the dielectric model may be used to describe the associated energy-loss processes.

2. *Case of 151 keV/A molecular ions on SiO_2*

A similar analysis was performed in Ref. [12] for 151-keV molecular ions in SiO_2. At this lower velocity, the contribution of core electrons to H^+ stopping is smaller: Valence electrons contribute to 94% of the total stopping.

3. *ELF*

We used experimentally measured ELFs for SiO_2 and Si_3N_4, which were fitted by Drude-type functions [27] (see Appendix B).

E. Multiple scattering

Multiple scattering has a significant influence on the evolution with penetration depth z of the distance R_{ij} between the nuclei of molecules. In Appendix C, we discuss how MS was taken into account in our calculations.

We present in Figs. 5 and 6 calculations of the evolution with z of the mean value of R_{ij}, with and without MS, for H_2^+ and H_3^+ ions in Si_3N_4.

The relative influence of MS on the mean distance $\langle R_{ij}\rangle$ is smaller for H_3^+ than for H_2^+ since MS is the same (same velocity) and since the repulsive force is much larger for H_3^+. In both cases, MS plays a major role in the evolution of the exploding molecule and could in no way be omitted.

F. Energy fluctuations

The two main sources of energy fluctuations are (a) the energy loss straggling and (b) the velocity fluctuations induced by Coulomb explosion. One must also consider (c) the incident beam energy fluctuations and (d) thermal vibration in the molecule. Other sources of energy fluctuations, described in Appendix D, are (e) velocity fluctuations induced by initial distance R_0 fluctuations and (f) MS.

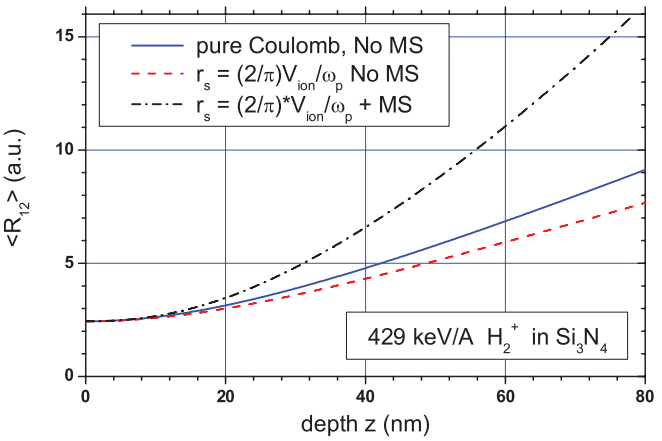

FIG. 5. (Color online) Mean distance $\langle R_{12}\rangle$ between nuclei in an exploding H_2^+ molecule. Calculation for pure Coulomb and screened potential, including or not MS.

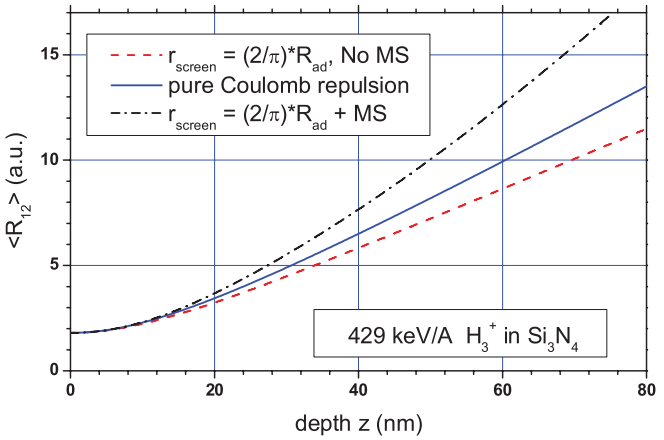

FIG. 6. (Color online) Mean distance $\langle R_{12}\rangle$ between nuclei in an exploding H_3^+ molecule. Calculation for pure Coulomb and screened potential, including or not MS.

(a) From Sec. II D, we observe that violent collisions on target electrons lead to a Gaussian energy loss spread at large depths. At small and even medium z values, a more involved non-Gaussian description is needed. For protons, we have used the full stochastic approach of the code SPACES [15] in Sec. II D, but for molecular ions, this code needs deep modification in order to include vicinage. We hence used the analytical approximations of [28] in our calculation code.

(b) In the c.m. frame, Coulomb explosion results in a repulsion velocity $\mathbf{V}$ for a given nucleus in the molecule. In the laboratory frame, the kinetic energy of this nucleus is $E_{\text{kin}} = (1/2)M_p(\mathbf{V}_{\text{ion}} + \mathbf{V})^2$, which, to first order in V, may be written

$$E_{\text{kin}} \simeq E_{\text{ion}} + M_p \mathbf{V}_{\text{ion}} \cdot \mathbf{V},$$

where E_{ion} is the kinetic energy for no Coulomb repulsion. Energy fluctuations originate then from the cross term (scalar product)

$$M_p \mathbf{V}_{\text{ion}} \cdot \mathbf{V} = M_p V_{\text{ion}} V_z = E_z,$$

where V_z is the projection of the repulsive velocity on the beam direction. For isotropically oriented molecules, $\mathbf{V}$ is isotropically distributed. Its projection is $V_z = V\cos\theta$, where θ is a random variable with a distribution $P(\theta)$ given by Eq. (A1). The probability distribution $f_u(u)$ of $u = \cos\theta$ is such that $f_u(u)du = P(\theta)d\theta = \sin\theta d\theta$: u is uniformly distributed on $[-1,1]$. Hence, for given V, V_z is a random variable uniformly distributed over $[-V,V]$. This is also the case for E_z, which is uniformly distributed:

$$P(E_z;V) = \begin{cases} [1/(2E_V)] & E_z \in [-E_V, E_V], \\ 0 & E_z \ni [-E_V, E_V], \end{cases} \tag{7}$$

where $E_V = M_p V_{\text{ion}} V$. V increases with depth z; at large depth z, V takes a constant value (no more repulsion at large distance). This limit velocity V^{lim} may be estimated using

energy conservation (strictly valid for zero MS). Consider the case of H_3^+ with initial distance $R_0 = 1.8$ a.u. and a pure Coulomb repulsion: One obtains $M_p(V^{\lim})^2 = 2/R_0$, which gives $M_p V_{\rm ion} V^{\lim} \simeq 5$ keV, that is, an energy distribution for E_z with a 10 keV width FWHM. Such very large fluctuations overshadow the collision fluctuations and strongly influence the shape of the yield curve $Y(E_b)$.

(c) The beam energy fluctuations for H^+ are Gaussian with standard deviation σ_b. For Si_3N_4 (see Sec. II D), $\sigma_b = 106$ eV. These measured fluctuations are greater than the fluctuations in the accelerating voltage, whose standard deviation was measured via a calibrated capacitive pickoff plate to be of similar magnitude and smaller than 40 eV for acceleration of H^+, H_2^+, and H_3^+ at 429 keV, 858 keV, and 1.29 MeV, respectively. For molecular ions the incident beam energy fluctuations are shared between the nuclei of the molecule. It thus appears reasonable to assume that both for H_2^+ and for H_3^+, σ_b does not exceed the value measured for H^+.

(d) For H_2^+ and H_3^+ ions, the initial slope of the experimental yield curve depends both on the incident beam energy fluctuations characterized by σ_b and on the velocity fluctuations brought by thermal vibrations in the incident molecule. As for the Coulomb explosion, the kinetic energy of nuclei entering the target is sensitive to a cross term $M_p V_{\rm ion} v_z^{\rm vib}$, where $v_z^{\rm vib}$ is the projection of the thermal velocity of a nucleus on the beam direction. When averaging over all molecule orientations, the law of this cross term is only approximately Gaussian (a Gaussian law is, however, assumed in what follows). It is possible to fit the initial slope of the yield curves $Y(E_b)$ for H_2^+ and H_3^+ molecules with the same parameters as for H^+, by only replacing σ_b by $\sigma_{bv} > \sigma_b$. In fact, whatever the hypothesis on σ_b, its value is in all cases small compared to σ_{bv} and it is then possible to extract from the experimental results a rather precise estimation of the thermal kinetic energy in the H_2^+ and H_3^+ molecules.

G. Screened Coulomb explosion and multiple scattering

After dissociation, the repulsive potential between the nuclei indexed by i and j in a molecule is assumed to be isotropic with an exponential screening function:

$$V(R_{ij}) = (Z_i Z_j / R_{ij}) \exp(-R_{ij}/r_s), \tag{8}$$

where r_s is a dynamic screening radius of the order of the adiabatic cutoff $R_{\rm ad}$ [29,30], R_{ij} is the distance between nuclei, and Z_i and Z_j are their atomic numbers (here 1). In the calculations, r_s is considered as a phenomenological parameter; its value is determined by fitting the experimental yield curves, with possible different screening radii for H_2^+ and H_3^+. When looking for the best fit, increasing r_s (less screening) leads to higher limit velocities $V^{\lim}$, thus to higher energy fluctuations, in particular at large depths. It also leads to a faster explosion of the molecules (vicinage disappears at smaller depths). Hence, the entire yield curve is affected by changing the screening, which is then a major issue in our experiments. Examples of Coulomb explosion kinematics for screened and unscreened potential were presented in Figs. 5 and 6.

Multiple scattering tends to increase the distance R_{ij} without changing the repelling velocity. Consequently, the Coulomb explosion velocity is smaller than that given by the conservation laws of mechanics when MS is included. For H_3^+, the reduction of the velocity is negligible, due to the strong repelling force. This is not the case for H_2^+, as shown in Fig. 7, which gives the evolution of the mean absolute value $\langle |V_z| \rangle$ of the repelling velocity projected on the beam direction, for a set of isotropically distributed H_2^+ molecules in Si_3N_4 (the figure considers a screened and an unscreened potential): MS tends to lower $|V_z|$.

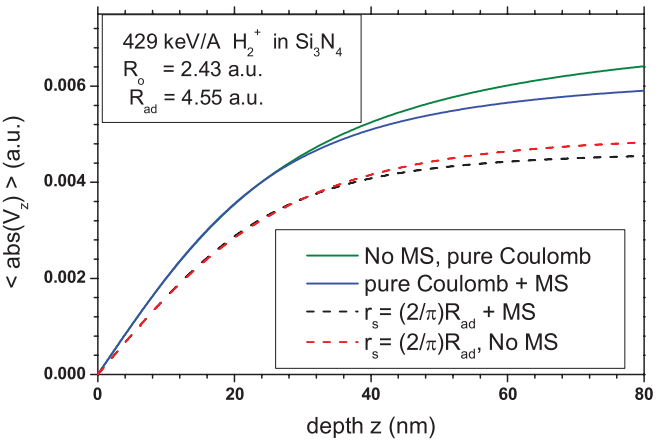

FIG. 7. (Color online) Influence of MS on the dynamics of Coulomb explosion for H_2^+ in Si_3N_4. V_z is the projection of the velocity of a nucleus in the molecular frame on the beam direction.

H. Vicinage effect as a function of R_{ij}: Influence of MS

Using Eq. (3) for istotropically oriented molecules, with various ELFs (SP, ELFs of Refs. [31–33]), one may determine the vicinage effect for valence electrons by numerical integration. We have taken into account the fact that core electrons contribute to the mean energy loss (18% in Si_3N_4, 6% in SiO_2), but do not contribute to vicinage for molecular ions. The vicinage effect described by the ratio $\chi_n = (S_{\rm vicin}/S_0)_{\rm tot}$ (the index "tot" indicating that core electrons are taken into account) as a function of the distance R_{ij} between nuclei, is represented in Figs. 8 and 9, respectively, for 429 keV/A H_2^+ and H_3^+ in Si_3N_4. As expected, since the ELF is rather narrow, the calculated curves are close to each other, even in the SP approximation (which leads to the strongest oscillations). For SiO_2, since the ELF peak is broader, a much larger difference shows up when comparing calculations performed in the SP approximation and with a more realistic ELF [12].

When neglecting MS, one may easily calculate the vicinage effect as a function of time or depth, by using the kinematics [$R_{ij}(t)$ or $R_{ij}(z)$ are determinist laws]. Calculations are more involved when including MS. We operate as follows. A set of repartition functions $F(R_{ij}; z_k)$ of the distance R_{ij} at given depths z_k are calculated by Monte Carlo for a given screening radius r_s [$F(R_{ij}; z_k)$ is the probability to find the internuclear distance below R_{ij}]. Examples of such repartition functions are given in Fig. 10 for H_2^+ and in Fig. 11 for H_3^+, in Si_3N_4. These curves were calculated for the large screening radius $r_s = 2R_{\rm ad} = 9.3$ a.u.

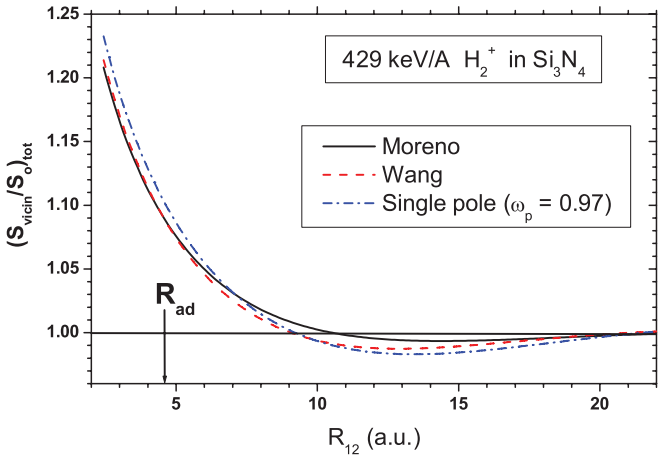

FIG. 8. (Color online) Vicinage effect $\chi_2 = (S_{\text{vicin}}/S_0)_{\text{tot}}$ for H_2^+ in Si_3N_4 as a function of the distance between nuclei, calculated for three different ELFs.

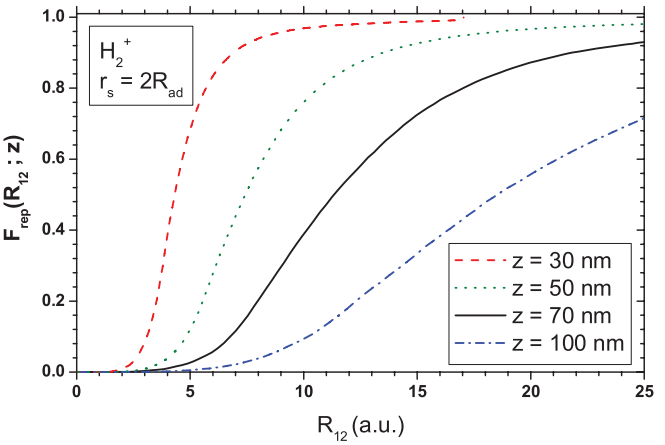

FIG. 10. (Color online) For H_2^+ in Si_3N_4, repartition function of the distance between nuclei calculated for four different depths z_i.

According to Figs. 8 and 9, vicinage effect disappears (or becomes smaller than 1) for $R_{ij} \gtrsim 2R_{\text{ad}}$. For H_3^+, considering only mean values, even for rather strong screening (see Fig. 6), the mean internuclear distance $\langle R_{ij} \rangle$ is larger than $2R_{\text{ad}}$ at depth $z = 50$ nm (MS included). One is then led to conclude that the vicinage effect is negligible at this depth. In fact, this conclusion is wrong because, due to MS, the $\langle R_{ij} \rangle$ are random variables. One may notice in Fig. 11 that at $z = 50$ nm about 50% of the R_{ij} are below $2R_{\text{ad}}$, and the corresponding molecules thus experience a vicinage effect, while for the remaining 50% the vicinage effect is negligible: Adding the two contributions, the overall result is a non-negligible effect. Hence, if one analyzes the influence of MS on the vicinage effect, (i) it increases the R_{ij} mean value, which tends to reduce the vicinage effect, but, (ii) at the same time, the very large R_{ij} fluctuations favor the vicinage effect. In the calculation code, at given depth z, $z_k < z < z_{k+1}$, one determines the vicinage effect by sampling the internuclear distances according to the set of repartition curves (an interpolation between curves indexed by k and $k + 1$ is performed). The vicinage effect as a function of depth for $r_s = (2/\pi)R_{\text{ad}}$ and different ELF (SP, Ref. [31]), including or not MS, is represented in Figs. 12 and 13, respectively, for H_2^+ and H_3^+ in Si_3N_4. Similar curves are obtained for SiO_2 (see $1/\chi$ in Fig. 2 of [12]). On Figs. 12 and 13, one can notice the following.

(i) As already pointed out in Ref. [12], MS suppresses the oscillating behavior with R_{ij} of the vicinage effect.

(ii) The relative influence of MS is larger for H_2^+ than for H_3^+.

(iii) For Si_3N_4, the difference between the crude SP approximation and the more elaborated ELF of [31] is weaker than for SiO_2 (see Fig. 2 of [12]).

(iv) For the chosen value $r_s = (2/\pi)R_{\text{ad}}$, the vicinage effect disappears at $z \approx 80$ nm for H_2^+ and at the lower value $z \approx 60$ nm for H_3^+. This result was expectable, as the repulsive potential experienced is stronger for H_3^+ than for H_2^+ ions. It is, however, in apparent contradiction with the experimental yield curves. The reason for this is analyzed in Sec. III I. There we will show that the shape of the experimental yield curves is strongly affected by the fluctuations of the depths at which the penetrating nuclei reach E_R.

When comparing the results presented in Figs. 12 and 13 for Si_3N_4 to those shown in Ref. [12] for SiO_2, one can notice that the vicinage effect for 151 keV/A molecules in SiO_2

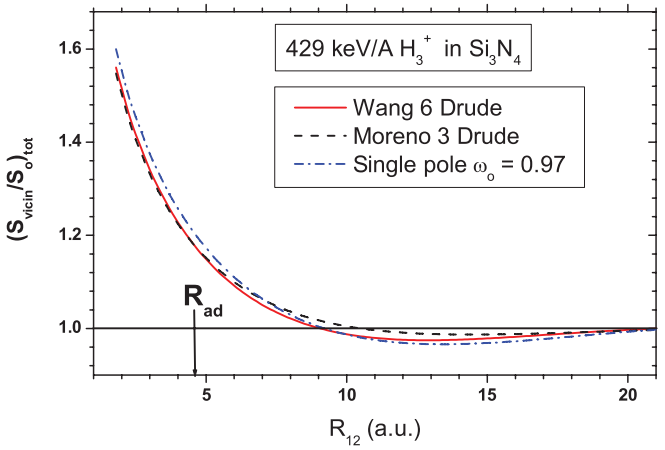

FIG. 9. (Color online) Vicinage effect $\chi_3 = (S_{\text{vicin}}/S_0)_{\text{tot}}$ for H_3^+ in Si_3N_4 as a function of the distance between nuclei, calculated for three different ELFs.

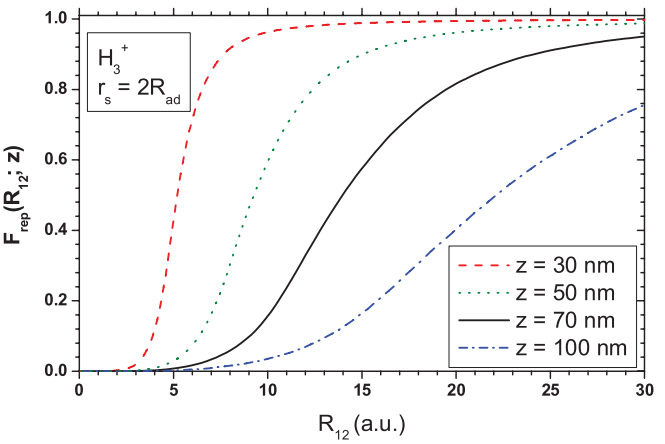

FIG. 11. (Color online) For H_3^+ in Si_3N_4, repartition function of the distance between nuclei calculated for four different depths z_i.

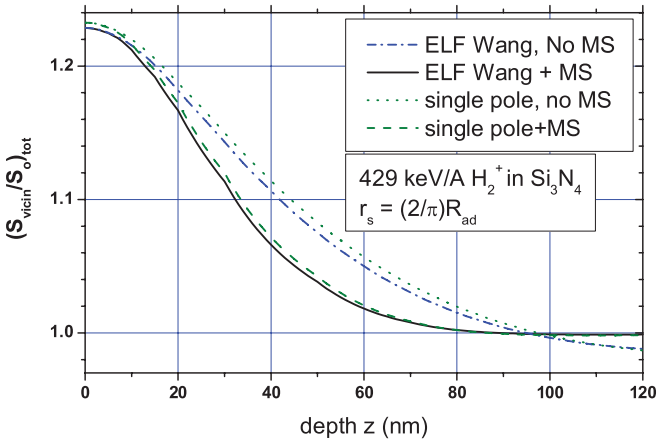

FIG. 12. (Color online) Vicinage effect $\chi_2 = (S_{\text{vicin}}/S_0)_{\text{tot}}$ for H_2^+ in Si_3N_4 calculated as a function of depth, when including or not MS.

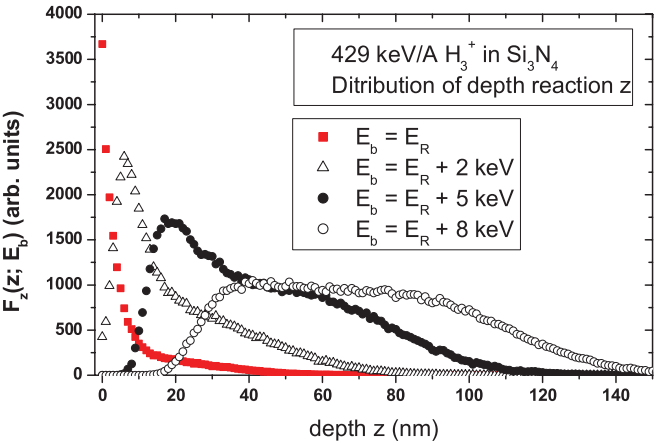

FIG. 14. (Color online) Distribution $F_z(z; E_b)$ of depth z where nuclei of H_3^+ molecules reach the resonance energy $E_R = 429$ keV, for various beam incident energies E_b.

is slightly lower than for 429 keV/A molecules in nitride: For H_3^+ in SiO_2, at the sample surface, $\chi_3(0) \simeq 1.53$ to be compared to 1.60 for the nitride experiment.

I. Fluctuations of the depth z at the resonance

For isotropically distributed incident molecules with given energy per nucleon $E_b > E_R$, the problem is to determine the distribution of depths $F_z(z; E_b)$ at which the nuclei reach the resonance energy. The calculations were performed by Monte Carlo using the approximations described above in this section. We consider the case of H_3^+ molecules (large Coulomb repulsion velocity) in Si_3N_4 (large ion velocity, i.e., large-velocity cross term). In Fig. 14, four different incident energies E_b are considered. The distributions broaden very rapidly when increasing E_b, mainly because Coulomb explosion generates a dramatic increase of the z fluctuations. In Fig. 1, the H_3^+ γ yield for $E_b = E_R + 8$ keV $= 437$ keV/A is significantly below the H^+ plateau level, a consequence of the vicinage effect. According to Fig. 3, the corresponding *mean* depth at which the energy E_R is reached for this value of E_b is ≈60 nm [A more precise determination of this mean depth is obtained from the mean value of the distribution $F_z(z; E_b = 437$ keV) in Fig. 14: We find then 70 nm.] As we

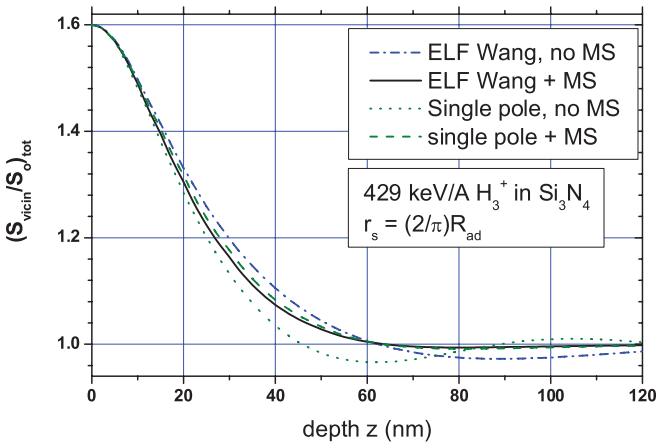

FIG. 13. (Color online) Vicinage effect $\chi_3 = (S_{\text{vicin}}/S_0)_{\text{tot}}$ for H_3^+ in Si_3N_4 calculated as a function of depth, when including or not MS.

have determined (see Fig. 13), that there is no more vicinage effect beyond 60 nm, we must conclude that the vicinage effect cannot simply be related to the mean depth. This results from the very broad distribution $F_z(z; E_b = 437$ keV). The latter extends from ≈20 nm to more than 130 nm and, for the part of the distribution corresponding to 20 nm $< z <$ 60 nm, there is indeed a vicinage effect, which is responsible for the γ yields significantly smaller than 1 that we observe experimentally. This is a key point in our experiment: Due to very strong energy fluctuations caused by Coulomb explosion, the γ yield in the Si_3N_4 experiment (Fig. 3), or the α yield in the SiO_2 experiment, do not give a direct image of the evolution of the vicinage effect with depth $\chi(z)$. Elaborate calculations are needed to extract $\chi(z)$ from the experimental results.

Furthermore, the energy fluctuations also affect the measured yields independently of the vicinage effect. The very broad distribution $F_z(z; E_b = 437$ keV) clearly shows that the nuclei have experienced very different histories: The mean kinetic energy variation of an ion reaching E_R at 20 nm is 6 times higher than that of an ion for which E_R is reached at 120 nm. The reason for this is that during the Coulomb explosion, some nuclei of the molecule are accelerated, while others are decelerated. In fact, we are interested in the local stopping power $\delta E/\delta z$ of the nuclei when they reach E_R, since the γ yield is inversely proportional to this. An ion reaching E_R at depth greater than 60–70 nm is no longer subjected to a repulsive potential and thus no longer accelerated or decelerated: It thus experiences the usual stopping power of an "ordinary" monatomic ion and has the same contribution to the γ yield. In contrast, an ion reaching E_R at depths smaller than 60–70 nm will not only still be subject to the vicinage effect but will also still be decelerated by the Coulomb explosion. Its stopping power will then be increased for these two reasons, resulting in a significant decrease of the γ yield.

A classical application of narrow resonances in NRA, is the possibility to determine concentration profiles of given isotopes in a target with very high depth resolution, by measuring yield curves around a narrow resonance, using monatomic beams. The depth resolution decreases at increasing depths due to the increase of the energy spread of the beam. In

principle, the use of molecular beams for depth profiling could be of interest. They may in particular provide high incoming nuclei densities and allow the use of electrostatic accelerators for which the minimum operating potential is greater than E_R. It may also be thought to use molecular ions in high-resolution medium energy backscattering experiments (MEIS). In fact, the very broad energy distributions reached by molecular ions in the first nm of their path, in connection with Coulomb explosion does not leave much hope to achieve high resolution depth profiling. Even close to the sample surface, the depth resolution is degraded by the thermal vibrations in the molecules.

J. Yield curve calculation

The yields $Y(E_b)$ obtained when scanning the beam energy E_b may be expressed as

$$Y(E_b) = K \int dE \sigma_R(E) \int dz C(z) g(E; E_b; z), \tag{9}$$

where $g(E; E_b; z)dE$ is the probability for a proton to have an energy in the interval $[E, E + dE]$ at depth z, for an incident energy E_b; $\sigma_R(E)$ is the nuclear cross section, centered on E_R and K a constant.

A nearly equivalent formulation consists in assuming a Dirac type cross section at $E = E_R$, $\sigma_R(E) = A_R \delta(E_R)$, and transferring the real shape of $\sigma_R(E)$ into $g(E; E_b; z)$ as independent energy fluctuations of the protons at depth z, with a Lorentzian law. $Y(E_b)$ is hence given by a single integration on z,

$$Y(E_b) \simeq K A_R \int dz C(z) g(E; E_b; z). \tag{10}$$

For a nucleus (proton) of a molecular ion with mean impinging energy E_b per nucleon, the energy $E(z)$ at depth z is a random variable:

$$E(z) = E_b - \delta E_{\text{in}} - \delta E_{\text{coll}} + M_p V_{\text{ion}} V_z - \int_0^z S(R_{12}(z)) dz. \tag{11}$$

In this expression, δE_{in} is a random variable which includes the beam energy fluctuations, the energy fluctuations induced by thermal vibrations, and the shape of the resonance. The associated probability law is the convolution product of a Gaussian (standard deviation σ_{bv}) by a Lorentzian with FWHM Γ_R. δE_{coll} corresponds to the fluctuations of energy loss to target electrons (with a nearly Gaussian law at large z). $M_p V_{\text{ion}} V_z$ is associated with the Coulomb explosion: For a determinist variation of V_z with z the law is rectangular for isotropically oriented molecules [see Eq. (7)]. When including the fluctuations induced by the initial distance R_0 distribution, the law is approximately given by the convolution product of this rectangular law by a Gaussian with standard deviation $M_p V_{\text{ion}} \sigma_V$ (see Sec. III F and Appendix D). All these contributions originate from independent processes. The corresponding law for the sum is then given by convolution of the individual probability laws. The last term, $\int_0^z S(R_{12}(z))dz = \Delta(z)$ is an energy loss that to first order is a mean value. In fact, due to anisotropy of the vicinage effect, to thermal vibrations, and to MS, this energy loss embodies also some fluctuations, but we have shown in Sec. III that they may be neglected in all cases.

We approximate the energy fluctuations due to lateral spread by a Gaussian (see Appendix C) with standard deviation σ_{LS} (for a tilting angle 68° in Si_3N_4, $\sigma_{\text{LS}} = 0.35$ keV, see Fig. 24). These energy-loss fluctuations originate from path-length fluctuations. Assuming that the ^{15}N or ^{18}O concentration C_O is independent of z close to the layer-substrate interface, one may simulate these path-length fluctuations by introducing a variable concentration profile $C(z)$ at the layer-substrate interface given by the convolution product of a Gaussian by a rectangular profile:

$$C(z) = \frac{1}{2} C_O \left[1 + \text{Erf}\left(\frac{z_{\max} - z}{\sigma_z 2^{1/2}} \right) \right], \tag{12}$$

where $z_{\max}$ is the mean total traveled path and $\sigma_z = \sigma_{\text{LS}}/S_0$. Erf stands for the error function.

IV. FITTING THE EXPERIMENTAL YIELD CURVES

A. Fitting the leading edge: Initial velocity distribution of the nuclei associated with thermal vibration

The leading edge slope of $Y(E_b)$ is a measure of the velocity distribution of the nuclei in the impinging molecular ions. It was fitted assuming a Gaussian contribution for the energy fluctuations induced by thermal vibrations (see discussion below). Removing the beam energy fluctuations σ_b (assumed to be the same for the three ions used) from the σ_{bv} fitting parameter gives an energy standard deviation $\sigma_{\text{Es}} = M_p V_{\text{ion}} \sigma_{Vz}$ where σ_{Vz} is a standard deviation for the thermal velocity of a nucleus in the c.m. frame of the molecule, projected on the beam direction.

We first consider the H_2^+ molecule in Si_3N_4. Neglecting rotational modes, the molecule is a one-dimensional (1D) oscillator; we measure $\sigma_{\text{Es}} \simeq 0.40$ keV $= 14.7$ a.u ($\sigma_{bv} \simeq 0.42$ keV). Along the direction of the molecule axis, the velocity fluctuations $\sigma_{V_{\text{th}}}$ for a nucleus in the c.m. frame are Gaussian in the harmonic approximation. For a set of isotropically oriented molecules, the law $g(V_z)$ of the projection V_z is not Gaussian and may be calculated as follows. For a given V_{th}, the law of the projection V_z is given by Eq. (7) (rectangular law). Since V_{th} is Gaussian, the joint probability law $g(V_z, V_{\text{th}})$ for the couple V_z, V_{th} is given by

$$g(V_z, V_{\text{th}}) = \frac{1}{2V_{\text{th}}} [Y(V_z + V_{\text{th}}) - Y(V_z - V_{\text{th}})] \times \frac{2}{(2\pi)^{1/2} \sigma_{V_{\text{th}}}} \exp\left(-\frac{V_{\text{th}}^2}{2\sigma_{V_{\text{th}}}^2} \right), \tag{13}$$

where Y is the Heaviside unit step function. Integrating $g(V_z, V_{\text{th}})$ over V_{th} yields the $g_z(V_z)$ law. An example of such a projected distribution is given in Fig. 15. The projected law is not at all gaussian (g_z is infinite at the origin), but when convoluted by a rather narrow Gaussian (energy dispersion of the beam), the shape is much closer to that of a Gaussian.

We have compared fits of the leading edge using a full Gaussian approximation (standard deviation σ_{bv}) to an exact calculation using the exact shape of $g_z(E_z)$. One finds that good full Gaussian fits of the main part of the leading edge may be obtained in a broad range of σ_b values, which

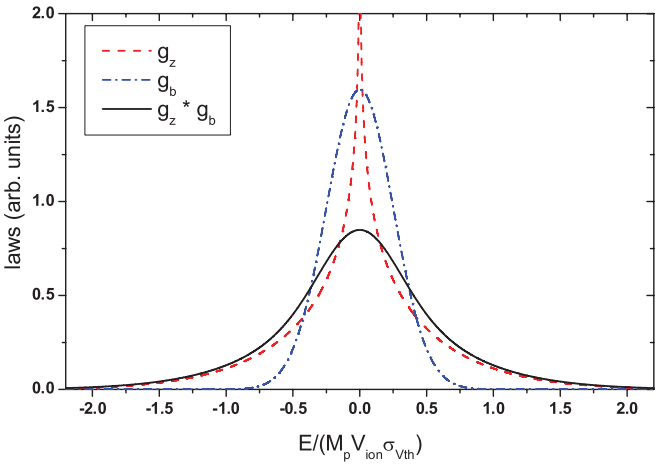

FIG. 15. (Color online) Red dashed line, law $g_z(E_z)$ of $M_p V_{\rm ion} V_z$ for isotropic H_2^+ harmonic oscillators with Gaussian velocity distribution (standard deviation $\sigma_{V_{\rm th}}$), and with velocity projection V_z on the beam direction; blue dot-dashed line, Gaussian beam energy dispersion g_b with standard deviation $M_p V_{\rm ion}\sigma_{V_{\rm th}}/4$; solid line, convolution of g_z with g_b.

includes those corresponding to our experiments, yielding a pseudovariance $\sigma_{\rm Es}^2 = \sigma_{bv}^2 - \sigma_b^2$. Moreover, the ratio between $\sigma_{\rm Es}$ and $M_p V_{\rm ion}\sigma_{V_{\rm th}}$ is found to be nearly constant, namely: $\sigma_{\rm Es} = 0.50 M_p V_{\rm ion}\sigma_{V_{\rm th}} \pm 2\%$ (note that in the case of 3D independent oscillators the ratio would be $1/\sqrt{3} = 0.577$). Thus, we are now able to extract the value of $\sigma_{V_{\rm th}}$ through a simple Gaussian fit of the leading edge of the excitation curves. Applying this procedure, we find $\sigma_{V_{\rm th}} \approx 0.003\,87$ a.u. The total kinetic energy in the molecule is hence $E_{\rm kin} = M_p\sigma_{V_{\rm th}}^2 \simeq 0.0275$ a.u. $= 0.75$ eV, larger than the 0.5 eV estimated from the Franck-Condon principle [22]. Keeping the harmonic oscillator approximation, the relation between $\sigma_{V_{\rm th}}$ and the standard deviation of the internuclear distance R_0 is $\sigma_{V_{\rm th}} = \omega\sigma_{R_o}$, ω being the characteristic vibration frequency. With the value $\omega = 0.2$ eV $= 0.007\,35$ a.u. proposed by Walters [22], we then obtain $\sigma_{R_0} = 0.53$ a.u. Comparing this value to the mean value $\langle R_0\rangle = 2.8$ a.u. measured in Ref. [21], we then get $\sigma_{R_0}/\langle R_0\rangle = 0.19$, a ratio only slightly lower than the value $\sigma_{R_0}/\langle R_0\rangle = 0.21$ that was measured in the latter reference.

For H_3^+, the analysis of the leading edge of the excitation curves provides $\sigma_{\rm Es} = 0.8$ keV. For this triatomic molecule, a full Gaussian approach with $\sigma_{\rm Es} = M_p V_{\rm ion}\sigma_{V_{\rm th}}/\sqrt{3}$ is justified. One finds $\sigma_{V_{\rm th}} \approx 0.0067$ a.u. (a value nearly twice that found in Ref. [34] for H_3^+ molecules cooled in a storage ring) and a total kinetic energy $E_{\rm kin} = (9/2)\sigma_{\rm Es}^2/(M_p V_{\rm ion}^2) = 0.124$ a.u. $= 3.4$ eV (0.041 a.u./nucleus). This corresponds to highly excited states since from [24], the characteristic frequency for this molecule is $\omega = 0.0137$ a.u. With this $E_{\rm kin}$ value, we obtain $\sigma_{R_0} = 0.49$ a.u. Considering the mean value $\langle R_0\rangle = 1.8$ a.u. measured in Ref. [23], we then get $\sigma_{R_0}/\langle R_0\rangle = 0.27$, which is significantly smaller than the value, larger than 0.4, that can be found in the literature [23]. We would then conclude that the H_3^+ ions produced in our experiment were less excited than those studied in Ref. [23]. However, the value of ω taken from [24] that we used to relate our measured $\sigma_{V_{\rm th}}$ to σ_{R_0} may well be an overestimation as it corresponds to the ground state, which is not the case for the molecules produced by the ion source. Thus, the discrepancy between our observations and the results obtained in Ref. [23] may be smaller than it appears at first sight.

In the SiO_2 experiment, the $\sigma_{\rm Es}$ are, respectively, 210 and 300 eV for H_2^+ and H_3^+. The corresponding kinetic energies in the molecules are 0.59 eV and 1.36 eV. These values are respectively slightly smaller, in the case of H_2^+, and much smaller in the case of H_3^+, than measured at 429 keV (respectively, 0.75 and 3.4 eV). This demonstrates that the conditions in the ion source play an important role on the excitation of the molecules. Whatever the laws connecting the vibrating velocities to the R_0 fluctuations, these fluctuations are smaller in the SiO_2 experiment than in the nitride experiment. In the frame of a simple harmonic oscillator model, the comparison of the values measured for $\sigma_{V_{\rm th}}$ respectively at 429 and 151 keV indicates that σ_{R_0} is 1.1 times lower in the case of H_2^+ ions and 1.6 times lower in the case of H_3^+ ions in the experiment performed at 151 keV than that performed at 429 keV.

To conclude this analysis, our study of the leading edge of the excitation curves show that for H_2^+ ions our results are in fair agreement with the R_0 distributions measured in Ref. [21], even if this agreement is slightly better for the experiments performed at 429 keV. We have thus decided to adopt these distributions when fitting the complete excitation curves obtained with H_2^+ ions in order to obtain information on the vicinage effect and on the dynamics of the Coulomb explosion. The situation is more complex for H_3^+ ions. In this case, there are serious uncertainties when attempting to deduce R_0 distributions from our experiments, even if it appears that the H_3^+ ions that we used are very probably significantly less excited than those studied in Ref. [23], in particular for our measurements at 151 keV. We have thus decided to systematically undertake two types of fits for H_3^+ ions. The first type of fit is obtained using the R_0 distributions of [23]. The second type of fit is obtained by setting for $\langle R_0\rangle$ the average between the value corresponding to the ground state and the value measured in Ref. [23] and by using a value for σ_{R_0} that is half that given in the literature. In the second type of fit we thus suppose that the molecules are much more weakly excited. Our aim is to determine the extent to which conclusions extracted from our measurements depend on the uncertainties related to the initial state of the molecules.

B. Fitting the whole yield curve: Determination of the vicinage effect and of the dynamics of Coulomb explosion

1. Si_3N_4

Calculations are based on the dielectric model. According to Sec. III, the detail of the narrow ELF function has moderate influence on the calculated vicinage for Si_3N_4. The influence of the thermal displacements (distribution of R_0) increases with depth and smooths the descending slope of the yield curve at the substrate interface. However, as seen in Appendix D, its influence is weaker than that of the collisional straggling, and this is even more the case in type 2 fits, where we consider narrower R_0 distributions. The parameter $\eta = 0.94$, which measures deviations from the Bohr free target electron model of the energy straggling induced by collisions on target electrons should not be varied. In fact, the main fitting

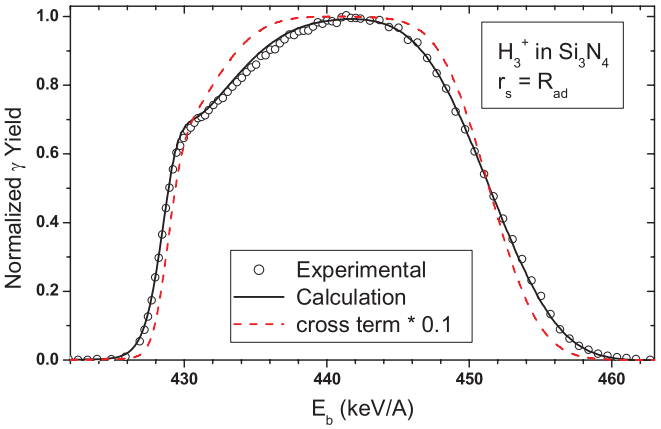

FIG. 16. (Color online) Fit of the yield curve for H_3^+ in Si_3N_4 using the ELF of [31], $\eta = 0.94$, including MS and the initial distance distribution of [23], with mean value $\langle R_0 \rangle = 1.8$ a.u. Open circles, experimental curve; solid curve, fit with the adjustable values $\sigma_{bv} = 800$ eV and $r_s = R_{ad}$; dashed curve, yield when lowering energy fluctuations (see text).

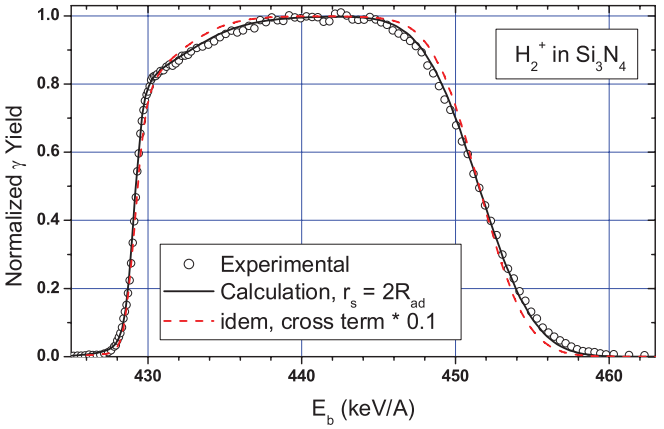

FIG. 17. (Color online) Fit of the yield curve for H_2^+ in Si_3N_4 using the ELF of [31], $\eta = 0.94$, including MS and the R_o distribution of [21]. Open circles, experimental curve; solid line, calculated yield with the adjustable values $\sigma_{bv} = 420$ eV and $r_s = 2R_{ad}$; dashed curve, yield when lowering energy fluctuations (see text).

parameter is the screening radius r_s. As shown in Sec. III, changing its value may change the shape of the yield curve $Y(E_b)$ over the whole incident beam energy range.

Looking for the optimum dynamic screening radius, we focus on the descending slope of $Y(E_b)$, since (i) it is governed by the limit value $V^{\lim}$ of the exploding velocity when particles are leaving the nitride layer and (ii) its shape is independent of the vicinage effect.

For H_3^+, in the case of a type 1 fit, an optimum adjustment of the descending slope fit is obtained with $r_s = R_{ad} = 4.65$ a.u. We notice in Fig. 16 that this also leads to a remarkable fit of the overall excitation curve. At first sight, this could appear surprising when considering Fig. 13, where the vicinage effect is calculated for a stronger screening [$r_s = (2/\pi)R_{ad}$], and does not extend beyond 60 nm: One could then expect for $r_s = R_{ad}$ no vicinage effect beyond depths of the order of $z_{vic} = 55$ nm, much smaller than the $\lambda_3^{vic} \simeq 90$ nm found experimentally for the γ yield $Y(E_b)$. In fact, according to the discussion in Sec. III I, we know now that, because of the fluctuations induced by the Coulomb explosion, the vicinage effect extends beyond z_{vic} on the yield curves. In order to illustrate the crucial influence of energy fluctuations, we have also represented in Fig. 16 the yield curve obtained when assuming that the velocity cross term $M_p V_{ion} V_z$ is divided by 10 with respect to its value obtained when considering isotropically oriented H_3^+ molecules. Such a situation would correspond to an experiment where incident molecules have been selected with a plane nearly perpendicular to the beam direction (low V_z projection). This reduction of the energy fluctuations profoundly modifies the yield curve. As expected, the calculated descending slope is very steep (small $V^{\lim}$). The shape of the vicinage region is also deeply affected and corresponds to what could be expected: For rather low energy fluctuations, a first-order analysis of the γ yield variations with mean depth is valid and $Y(E_b)$ reaches the plateau value (no vicinage) at rather shallow depths, a signature of the fast Coulomb explosion. Clearly, this first-order approach does not at all apply in our experiments.

We have also obtained a remarkable overall adjustment (not represented) of the excitation curve obtained with H_3^+ ions at 429 keV when attempting a type 2 fit. To get this agreement, we had to use a screening radius $r_s \approx 0.9R_{ad}$. This 10% difference with the r_s value used in the type 1 fit sets the uncertainty on the repulsive potential induced by our uncertainties on the initial condition of the H_3^+ molecules.

We now consider the case of H_2^+. We use the R_0 distribution of [21], with $\langle R_o \rangle = 2.8$ a.u. and leading to $\sigma_V = 0.23V(z)$ (see Appendix D). As shown in Fig. 17, with this distribution, a very large screening radius $r_s = 2R_{ad}$ had to be used in order to obtain a fair adjustment of the high energy descending slope of the yield curve. However, the calculated slope remains slightly steeper than the experimental one. This could be corrected for by slightly increasing $V^{\lim}$, and thus the energy fluctuations associated with the explosion. As we have already used a nearly unscreened repulsive potential, an increase of $V^{\lim}$ can only be obtained by slightly lowering the mean distance $\langle R_0 \rangle$ between the two nuclei of the molecule at the target entrance. Let us recall that we have adopted for R_0 the value measured in Ref. [21] which appeared quite consistent with our analysis of the leading edge of the excitation curves (see Sec. IV A). This value of R_0 is thus perhaps slightly overestimated. The fast Coulomb explosion is compensated for by the corresponding energy fluctuations caused by Coulomb explosion, and the yield $Y(E_b)$ variations are very well reproduced in the vicinage region. As in Fig. 16, in order to illustrate the influence of energy fluctuations on the shape of $Y(E_b)$, a dotted curve was calculated when lowering by a factor of 10 the velocity cross term valid for isotropically oriented incident molecules (see Fig. 17). The shape modification is here less marked than for H_3^+, indicating that the experiment with H_2^+ is less sensitive to the adjustable r_s value than the corresponding experiment with H_3^+.

We note that the isotopic exchange at the sample surface has a non-negligible influence on the shape of the calculated $Y(E_b)$ at the top of the leading edge ($E_b \approx 430$ keV), mainly for H_3^+ (a more pronounced bump appears for zero exchange). However, the exchange parameters carefully determined from

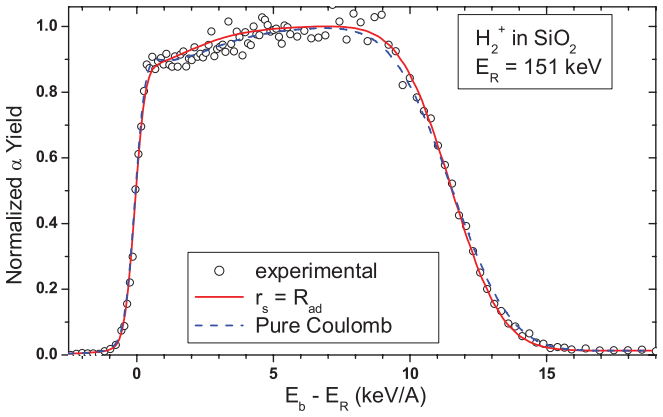

FIG. 18. (Color online) Fit of the yield curve for H_2^+ in SiO_2 using the ELF of [35], $\eta = 0.80$, including MS and R_o distribution of [21]. Open circles, experimental curve; solid curve, fit with $\sigma_{bv} = 235$ eV and $r_s = R_{ad}$; dotted red curve, pure Coulomb repulsive potential.

the H^+ yield curve play a negligible role on the main fitting parameters (r_s, ELF, σ_{bv}, $\langle R_0 \rangle$).

2. SiO_2

Preliminary fits were presented in Ref. [12] for the experiment performed in SiO_2. We reconsider here these fits keeping in mind the very important role of energy fluctuations. Since the two materials used in our experiment are both insulators with rather close valence electron density, one may anticipate rather similar screening for the Coulomb explosion. We used the same approach for the fitting as that used for the experiment in nitride, that is, looking for the best r_s when fitting the high energy edge, with the R_0 distribution of the literature. We show in Figs. 18 and 19 calculated curves obtained for type 1 fits, that is, when using the R_0 distributions of the literature. In order to estimate the sensitivity of the fits to the screening radius, we present in both figures two curves, calculated respectively with $r_s = R_{ad}$, or in the case of pure Coulomb repulsion (r_s infinite). In fact, for H_2^+, due to the statistics and the poor sensitivity of the yield curve to the screening radius, it is hardly possible to decide between $r_s = R_{ad}$ and $2R_{ad}$. On the other hand, for H_3^+, $r_s = R_{ad}$ gives rather clearly the best fit in the two regions of interest. We have also obtained a type 2 fit for H_3^+ ions (using smaller $\langle R_0 \rangle$ and narrower R_0 distributions than in the literature; see Sec. IV A), and, like for the experiment performed at 429 keV, we note that the best agreement is obtained by reducing r_s by ≈10%, that is, by setting $r_s = 0.9R_{ad}$.

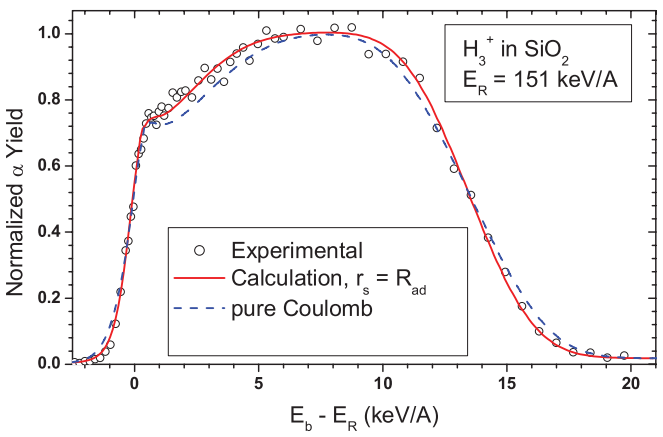

FIG. 19. (Color online) Fit of the yield curve for H_3^+ in SiO_2 using the ELF of [35], $\eta = 0.80$, including MS and the R_o distribution of [23]. Open circles, experimental curve; solid curve, fit with $\sigma_{bv} = 320$ eV and $r_s = R_{ad}$; dotted red curve, pure Coulomb potential.

C. Fluctuations of the stopping power

When comparing $Y(E_b)$ for the two sets of experiments, one observes that the vicinage effect seems greater for Si_3N_4 than for SiO_2. In fact, the theory predicts rather close vicinage effects for $R_{ij} \approx R_o$. This apparent contradiction originates from fluctuations in the stopping power induced by the acceleration and deceleration effects discussed in Sec. III I, where we showed that they tend to further lower the yield curves in the vicinage region. The stopping power is higher for protons at 151 keV (experiment in SiO_2) than at 429 keV (experiment in Si_3N_4). Then the relative stopping power fluctuations are stronger in the nitride experiment and we thus expect a stronger influence on the yield curves.

V. CONCLUSION

A. Screening

We have performed a detailed analysis of all the contributions to energy-loss fluctuation, including the influence of the R_0 distribution. Due to our incomplete knowledge of this distribution, the screening radius r_s extracted from our experiments bears some relative uncertainties, in the 10% to 20% range. For the nitride experiment, r_s is found unambiguously larger for H_2^+ than for H_3^+, typically $2R_{ad}$ against R_{ad}. For the SiO_2 experiment, we find again, that for H_3^+ ions the value of r_s is close to R_{ad}. For H_2^+ ions the sensitivity to r_s is poorer, and our results can be fitted with r_s values lying in the $[R_{ad}, 2R_{ad}]$ range. Thus, even if there are serious uncertainties on the value of r_s for H_2^+ at 151 keV/A, we are led to conclude (i) that the repulsive potential is more screened for H_3^+ than for H_2^+ ions, and that for the latter the screening is very weak, and (ii) that r_s, like R_{ad}, scales with V_{ion}.

B. Vicinage effect, electron gas model

Silicon nitride is a nearly ideal medium concerning the response of its valence gas to a fast moving charge, as it presents a narrow single-peaked ELF. Moreover, the experiment is performed in a high velocity regime (429 keV/A), in a medium with low atomic number (mean value 10). The experiment is hence not very sensitive to the precise shape of the ELF and a simple representation of the ELF by sums of Drude functions is more than sufficient. As shown, the confrontation between the dielectric model and the experiment is not direct since energy fluctuations and Coulomb explosion kinematics contribute to the shape of $Y(E_b)$ in the vicinage region. Since the fluctuations are smallest close to the layer surface, the most severe test of the dielectric model concerns internuclear distances R_{ij} close to the initial distance R_0,

that is, for $R_{ij} \approx 2$ a.u. $\approx R_{\rm ad}/2$. Having confidence in the screening radius r_s, the experiment with the nitride, performed with very good statistics, confirms the theoretical prediction of the dielectric model on the vicinage dependence with the internuclear distance, for $R_{\rm ad}/2 \lesssim R_{ij} \lesssim 2R_{\rm ad}$, with good precision. For the experiment at 151 keV/A in SiO_2, the perturbative approach of the dielectric model and the single Drude approximation for the ELF are less justified and from this point of view the experiment is a more severe test for these approximations. Considering the quality of the fits in Figs. 18 and 19, the theoretical approach used here seems justified.

C. Thermal vibrations

The fit of the leading edge of the yield curve provides the velocity distribution of the nuclei of the impinging molecular ions in the c.m. frame. The comparison of the results obtained, respectively, at 151 and 429 keV demonstrates that the levels of excitation reached by the molecules depend markedly on the conditions upon which they were produced in the ion source. We have tried, in a rather crude way, to relate the velocity distributions to the distributions of distances R_0 between the nuclei of a molecule. The knowledge of the latter, on which information can be found in the literature, is required to analyze our data related to vicinage effects and Coulomb explosion. Our conclusion is that, in the case of H_2^+, the R_0 distributions proposed in the literature are consistent with the initial velocity distributions that we measure. For H_3^+ ions, however, this is not the case; these ions are clearly less excited in our experiments than those analyzed in the literature, and we had to consider narrower R_0 distributions and smaller R_0 mean values.

D. Summary

(i) The Coulomb explosion in amorphous insulators such as Si_3N_4 and SiO_2 for protons clusters with energy of a few 100 keV/A is governed by a screened Coulomb potential with screening radius in the $R_{\rm ad}$ (for H_3^+ clusters) to $2R_{\rm ad}$ (for H_2^+ clusters) range.

(ii) The dielectric model using ELF described by Drude functions is pertinent to describe the vicinage effect.

(iii) The shape of the yield curves $Y(E_b)$ obtained when scanning the beam energy E_b is governed both by Coulomb explosion and vicinage effect. Energy fluctuations related to the Coulomb explosion play a major role in this shape.

(iv) As a consequence of the preceding point, the shape of $Y(E_b)$ does not give a direct image of the evolution of the vicinage effect with depth. Involved calculations are needed to extract this variation law.

(v) Molecular ion beams should not be used for high-resolution depth profiling using narrow nuclear resonances, unless a very careful analysis of all the causes of energy fluctuations is undertaken.

ACKNOWLEDGMENTS

We wish to thank E. Briand and H. Tancrez for providing molecular beams with high current and energy resolution, and P. Grande for enlightening discussions and suggestions.

APPENDIX A: ANISOTROPY OF VICINAGE EFFECT

Let us consider Eq. (5). For aligned H_2^+ molecules ($d = R_{12}$, $\rho = 0$), the interference term oscillates with no damping when d increases with depth; however, for H_2^+ molecules perpendicular to the beam direction ($d = 0$, $\rho = R_{12}$), the Bessel function introduces damping. One may estimate the energy fluctuations induced by anisotropy as follows.

(i) Calculate the mean distance $\langle R_{12}(z)\rangle$ between the nuclei as a function of depth. For this estimation, we used an initial mean distance $R_0 = 2.4$ and assumed that the explosion of the molecules was governed by an isotropic screened potential (Yukawa, with the screening radius $r_s = (2/\pi)R_{\rm ad}$ used in Ref. [12]), and we include MS.

(ii) Using $S_{\text{mol-SP}}(R_{12},\theta)$, for a given θ, calculate $S_{\text{mol-SP}}(\langle R_{12}(z)\rangle,\theta)$ at various depths $z \leqslant z_o$ to calculate the mean energy loss $\Delta E(z_o;\theta)$ over a given thickness z_o; repeat this procedure for various θ. The variations of $\Delta E(z_o;\theta)$ are represented in Fig. 20 for $z_o = 100$ nm in the case of 429 keV/A H_2^+ in Si_3N_4.

For isotropically oriented H_2^+ molecules, the probability distribution $P(\theta)$ of θ is given by

$$P(\theta) = (1/2)\sin\theta, \quad 0 < \theta < \pi. \tag{A1}$$

In Fig. 20, $\Delta E(z_o;\theta)$ is centered around the mean value $\langle\Delta E\rangle_{\rm iso}$ calculated according to the $P(\theta)$ law.

$P(\theta)$ favors the large angles. Moreover, except for a relatively small fraction of molecules which enter the target with values of θ small enough to allow the trapping of the second atom of the molecule by the wake potential created by the first one, MS induces independent lateral displacements of the two nuclei and hence induces a rapid rotation of the molecule (θ increases). Finally, we estimate that the energy-loss fluctuations induced by anisotropy are in all cases smaller than $\pm\approx$0.3 keV. This value is to be compared to the shape of the high-energy part of $Y_2(E_b)$ in Fig. 1: Energy fluctuations at large depths are of the order of $\approx$7 keV. This justifies the early average on the molecule orientation. This conclusion is also valid for H_3^+ molecules and for the SiO_2 target.

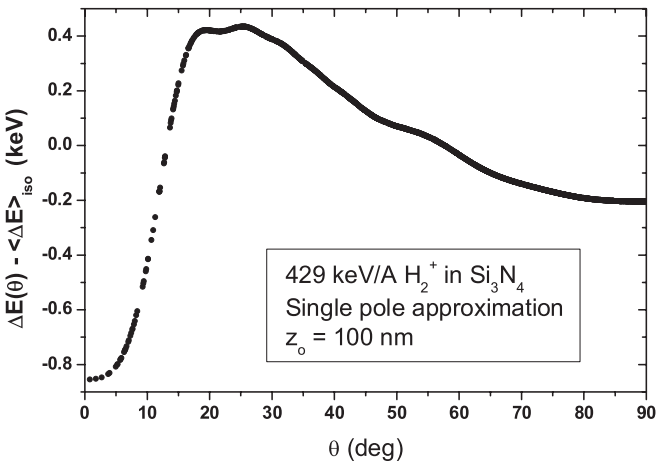

FIG. 20. Mean energy-loss variations $\Delta E(\theta)$ for a $z_o = 100$ nm path length, for 429 keV/A H_2^+ molecules in Si_3N_4 as a function of their orientation θ with respect to the beam direction. $\Delta E(\theta)$ is centered on the isotropic mean energy loss $\langle\Delta E\rangle_{\rm iso} = 10.4$ keV.

APPENDIX B: ELECTRON LOSS FUNCTION

1. Si_3N_4

All the information on the target valence electrons is embodied in the ELF, which must satisfy the sum rule $\int_0^\infty d\omega\omega \mathrm{Im}[-1/\epsilon(q,\omega)] = \overline{\omega}_{\mathrm{elf}} = 2\pi^2 n_e = 1.25$ for all q ($n_e = 0.0632$). Experimental values of ELF at $q \simeq 0$ are available (UV optical measurements, typically up to $\omega \lesssim 2$ a.u.). Starting from measured $\mathrm{Im}[-1/\epsilon(q=0,\omega)]$, a theory is then needed to extend these experimental data to all q values. For amorphous Si_3N_4, from [32], as quoted by [33], the ELF is a single peak, with maximum value ≈2.02, corresponding to $\omega_{\text{p-exp}} = 0.92$ a.u., with a width (FWHM) 0.32 a.u., and a large tail toward high ω. The value of $\omega_{\text{p-exp}}$ is close to the plasma frequency $\omega_p = 0.89$ corresponding to $n_e = 32$ electron/molecule, partly justifying our core versus valence electron partition. In fact, the ELF close to its maximum value was not measured in Ref. [32] and was extrapolated in Ref. [33]. For this reason, we also consider the theoretical calculation of Wang *et al.* [31] for Spinel Si_3N_4, which predicts a narrower peak (0.14 a.u. FWHM) with a maximum value ≈6 corresponding to $\omega_{\text{p-exp}} = 0.99$. ELFs described by sums of Drude-type functions satisfy the above sum rule and are largely adequate to fit the narrow single-peaked ELF of Si_3N_4 [27]:

$$\omega \mathrm{Im}\left(\frac{-1}{\epsilon(q,\omega)}\right) = \frac{4\pi n_e \gamma \omega^2}{[(\omega_p + q^2/2)^2 + \gamma^2\omega^2]}. \qquad \text{(B1)}$$

The best overall agreement with [33] is obtained for a sum of 3 Drude functions ($i = 1,3$) with damping factors $\gamma(i) \simeq 0.3$, 0.8, 0.99 a.u., $\omega_p(i) \simeq 0.93$, 0.7, and 1.54 a.u., with weighing factors $A(i) = 0.73$, 0.145, and 0.125. For the ELF calculated in Ref. [31], six Drude functions were used ($i = 1,6$), $\gamma(i) \simeq 0.4$, 0.2, 0.085, 0.05, 0.05, 0.05 a.u., $\omega_p(i) \simeq 0.88$, 0.89, 0.992, 1.032, 1.062, 0.082, $A(i) = 0.12$, 0.06, 0.52, 0.13, 0.11, 0.06. These two ELF and their description using sums of Drude functions are represented in Figs. 21 and 22.

In a medium with a rather narrow single-peaked ELF, one may anticipate rather small differences in the calculated vicinage effect when changing from the ELF function of [33],

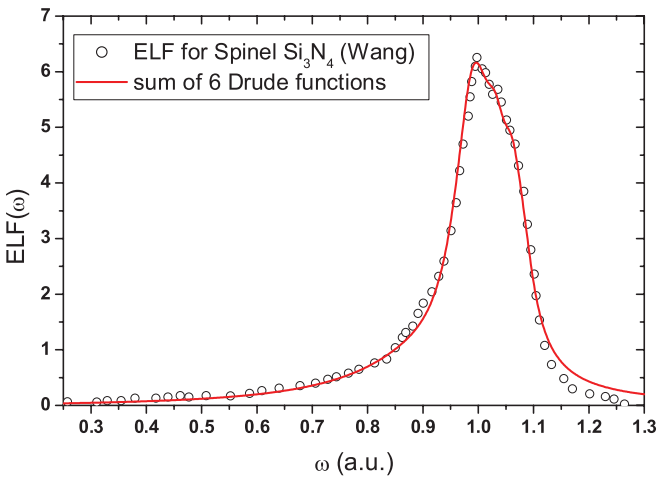

FIG. 21. (Color online) Open circles, ELF for Si_3N_4 as calculated by [31]; solid line, corresponding fit using a sum of six Drude functions.

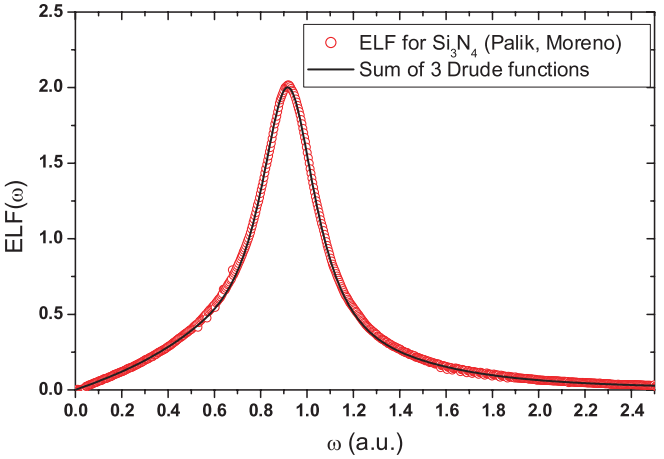

FIG. 22. (Color online) Open red circles, ELF for Si_3N_4 as measured by [32] and extrapolated by [33]; solid line, corresponding fit using a sum of three Drude functions.

to that of [31] or even to the SP description [Eq. (4)]. Since the Drude function may be expressed as the sum of two second-order rational fractions in ω, integration over ω in Eq. (3) is analytical and only one numerical integration, on q, is needed.

2. SiO_2

For SiO_2, the ELF is broader than for Si_3N_4. It exhibits oscillations and is approximated [12] by a single Drude function with damping factor $\gamma = 0.8$, and $\omega_p = 0.88$.

APPENDIX C: MULTIPLE SCATTERING

Multiple scattering is the consequence of successive small angular deflections of an incident ion by the target nuclei. Collisions of the incident protons on target nuclei are elastic and may be described using a classical description. The interaction potential is screened by the target electrons and a simple Thomas-Fermi type screening may be used, here the Lenz-Jensen [36] formulation. It has been shown [37,38] that MS in polyatomic targets may reduce to MS in a monatomic target with a mean atomic number $\overline{Z}$ which depends on the target thickness. For rather small and close atomic numbers (here 14 and 7 or 8), and rather thick targets, this mean value is close to the arithmetic mean value, that is, 10 for both Si_3N_4 and SiO_2. We consider that the target nuclei are randomly distributed in space and that trajectories are straight lines between the collisions. Using Monte Carlo one may easily simulate these random interactions.

In the present experiment, we are essentially interested in the lateral displacement ρ distribution of the incident nuclei. In the transverse plane, the successive collisions lead to 2D random vectors $\vec{\rho}_i$ corresponding to the lateral displacement between two successive collisions. For a given path length z, if N is the corresponding random number of collisions, one has $\vec{\rho} = \sum_{i=1}^{N} \vec{\rho}_i$. The impact parameters leading to significant angular deflections are small compared to an interatomic distance. Hence, except for molecules nearly aligned with the incident beam direction, that is, the minor fraction for which the second ion of the molecule (case of H_2^+) is trapped by

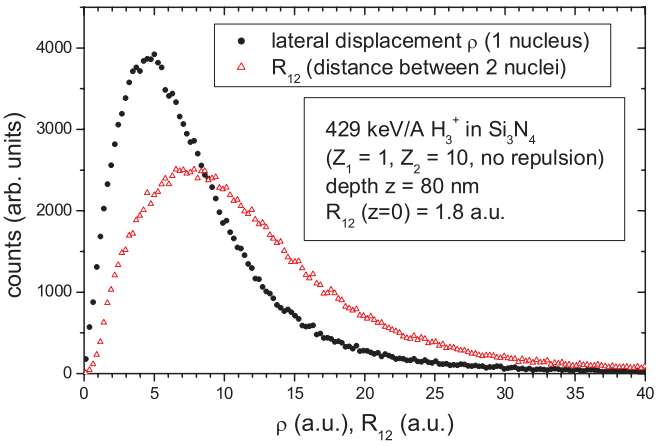

FIG. 23. (Color online) Lateral distribution ρ and distribution of the distance $R_{ij} = R_{12}$ between nuclei for 429 keV/A H_3^+ in Si_3N_4, at depth $z = 80$ nm. Monte Carlo calculation using a Lenz-Jensen screening function (Coulomb repulsion was omitted when calculating R_{12}).

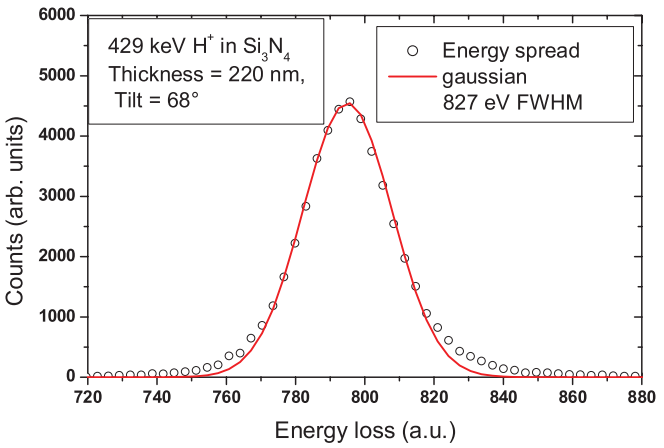

FIG. 24. (Color online) Monte Carlo calculation of the energy-loss fluctuations induced by lateral displacement in a tilted target (tilt = 68°), for 429-keV protons Si_3N_4 (mean path length 220 nm).

the wake potential along the beam direction, the deflections of the nuclei composing a molecular ion may be considered as independent: In the transverse plane, each nucleus follows an independent random walk.

In the Monte Carlo calculation, one may also calculate the evolution with z of the distance R_{ij} between two nuclei in a molecule (initial distance R_o). Repeating such a calculation for a larger number of molecules leads to distributions of the lateral displacement $\rho = \| \vec{\rho} \|$ for a nucleus and to the distribution of R_{ij}. In Fig. 23, we consider the case of 429 keV/A H_3^+ molecules at depth $z = 80$ nm in Si_3N_4. In this calculation, the initial distance $R_{ij} = R_0$ is fixed and there is no Coulomb repulsion between the nuclei of the molecule in order to isolate the specific contribution of MS.

The distribution of R_{12} (identical to that of R_{13} or R_{23}) is very broad and its mean value is very large compared to the initial distance $R_0 = 1.80$ a.u. Clearly, the MS plays a major role in this experiment. Small-angle MS scales as $1/E$, where E is the kinetic energy of the colliding monatomic ions (here a proton). The contribution of MS in the Si_3N_4 experiment is then smaller than in the experiment performed in SiO_2 [12] ($E = 151$ keV/A).

The experiments were performed on tilted targets. One hence has to consider the influence of the lateral displacement on the path lengths throughout the whole target [38,39] (for perpendicular targets, this is a second order effect). Using a Monte Carlo code, we obtain the result displayed on Fig. 24 for a Si_3N_4 target tilted at $\simeq 68°$ (mean traveled path $z_{\max} = 220$ nm). The path-length fluctuations around the mean value are converted into energy-loss fluctuations, via the proton stopping power (no vicinage effect at the nitride-substrate interface). This distribution is not Gaussian; the width FWHM $\simeq 0.83$ keV, is larger than the estimated width corresponding to anisotropy in the vicinage effect (see Fig. 20), but is still rather small compared to the major causes of energy fluctuations (Coulomb explosion, energy loss straggling). It was nevertheless included in all our calculations.

APPENDIX D: OTHER SOURCES OF ENERGY FLUCTUATIONS

1. Velocity fluctuations related to R_0 fluctuations

The discussion in Sec. III F (b) should now be extended in order to take into account the influence of the fluctuation of the initial internuclear distance R_0 due to thermal vibrations. For a given R_0 distribution and a given screening radius r_s, one may calculate the velocity distribution of the nuclei of an molecule in the c.m. frame at a given depth z. For H_2^+, using the asymmetrical distribution of [21], one finds an approximately Gaussian velocity distribution of standard deviation $\sigma_V(z) \simeq 0.23V(z)$, where $V(z)$ is the repulsive velocity of a nucleus in the c.m. frame. Similarly, for H_3^+, using [23], one finds $\sigma_V(z) \simeq 0.32V(z)$. The corresponding energy fluctuation for an incident nucleus is given by $\sigma_{ER_0} = M_p V_{\rm ion} \sigma_V$. At large depth, $V(z) = V^{\rm lim}$. An upper limit for $V^{\rm lim}$ is obtained when assuming that the repulsive potential between the nuclei of an initial molecule is unscreened. For H_3^+ ions, this upper limit is 0.0246 a.u, which leads, for a 429 keV/A incident beam, to an upper value of σ_{ER_0} equal to 60 a.u., to be compared to the collisional energy straggling $\Omega = 84.5$ at the nitride substrate interface: σ_{ER_0} is not negligible and was taken into account in all our calculations.

2. Energy-loss fluctuations induced by MS

Due to MS, from one molecule to another, the evolution of the distance $R_{ij}(z)$ between the nuclei varies. This in turn leads to fluctuations in the energy loss through the dependence with R_{ij} of the vicinage effect. Coulomb explosion and energy loss are correlated: Molecules having suffered high energy loss (due to vicinage) at given z are those with R_{ij} smaller than its mean value. For larger z, the small R_{ij} distance implies a stronger Coulomb repulsion and the further energy losses are smaller than the average value. Using a full Monte Carlo calculation, we have shown that these correlations play a minor role in all our experiments. Hence, we may use procedures that avoid time-consuming full Monte Carlo calculations (see in particular Sec. III H).

[1] J. W. Tape, W. M. Gibson, J. Remillieux, R. Lauber, and H. Wegner, Nucl. Instrum. Methods **132**, 75 (1976).
[2] E. Ray, R. Kirsch, H. H. Mikkelsen, J.-C. Poizat, and J. Remillieux, Nucl. Instrum. Methods Phys. Res., Sect. B **69**, 133 (1992).
[3] R. Garcia-Molina, C. D. Denton, F. J. Pérez-Pérez, I. Abril, and N. R. Arista, Phys. Status Solidi B **219**, 23 (2000).
[4] M. Behar, J. F. Dias, P. L. Grande, J. H. R. dos Santos, and N. R. Arista, Phys. Rev. A **64**, 022904 (2001).
[5] S. M. Shubeita, M. A. Sortica, P. L. Grande, J. F. Dias, and N. R. Arista, Phys. Rev. B **77**, 115327 (2008).
[6] J. Neufeld and R. H. Ritchie, Phys. Rev. **98**, 1632 (1955).
[7] W. Brandt and J. Reinheimer, Phys. Rev. B **2**, 3104 (1970).
[8] W. Brandt, A. Ratkowski, and R. H. Ritchie, Phys. Rev. Lett. **33**, 1325 (1974).
[9] N. R. Arista, Phys. Rev. B **18**, 1 (1978).
[10] G. Basbas and R. H. Ritchie, Phys. Rev. A **25**, 1943 (1982).
[11] N. R. Arista, Nucl. Instrum. Methods Phys. Res., Sect. B **164-165**, 108 (2000).
[12] A. L'Hoir, J. J. Ganem, I. Trimaille, and I. C. Vickridge, Nucl. Instrum. Methods Phys. Res., Sect. B **268**, 2850 (2010).
[13] G. Amsel and G. Samuel, J. Phys. Chem. Solids **23**, 1707 (1962).
[14] P. L. Grande and G. Schiwietz, Phys. Rev. A **58**, 3796 (1998).
[15] I. C. Vickridge and G. Amsel, Nucl. Instrum. Methods Phys. Res., Sect. B **45**, 6 (1990).
[16] G. Amsel and I. C. Vickridge, Nucl. Instrum. Methods Phys. Res., Sect. B **45**, 12 (1990).
[17] I. Vickridge and G. Amsel, Nucl. Instrum. Methods Phys. Res., Sect. B **64**, 687 (1992).
[18] B. Maurel and G. Amsel, Nucl. Instrum. Methods Phys. Res. **218**, 159 (1983).
[19] G. Amsel, C. Cohen, and B. Maurel, Nucl. Instrum. Methods Phys. Res., Sect. B **14**, 226 (1986).
[20] N. Bohr, Kgl. Dan. Vidensk. Selsk. Mat.-Fys. Medd. **18**, 8 (1948).
[21] E. P. Kanter, P. J. Cooney, D. S. Gemmell, Z. Vager, W. J. Pietsch, and B. J. Zabransky, Nucl. Instrum. Methods **170**, 87 (1980).
[22] W. L. Walters, D. G. Costello, J. G. Skofronick, D. W. Palmer, W. E. Kane, and R. G. Herb, Phys. Rev **125**, 2012 (1962).
[23] M. J. Gaillard, D. S. Gemmell, G. Goldring, I. Levine, W. J. Pietsch, J.-C. Poizat, A. J. Ratkowski, J. Remillieux, Z. Vager, and B. J. Zabransky, Phys. Rev. A **17**, 1797 (1978).
[24] L. Salmon and R. D. Poshusta, J. Chem. Phys. **59**, 3497 (1973).
[25] N. V. de Castro Faria, I. Borges Jr., L. F. S. Coelho, and G. Jalbert, Phys. Rev. A **51**, 3831 (1995).
[26] J. F. Ziegler, J. P. Biersack, and M. D. Ziegler, *SRIM—The Stopping and Range of Ions in Matter*, ISBN 0-9654207-1-X (Lulu Press, Morrisville USA, 2008).
[27] J. C. Ashley, J. J. Cowan, R. H. Ritchie, V. E. Anderson, and J. Hoelzl, Thin Solid Films **60**, 361 (1979).
[28] R. P. Pezzi, C. Krug, P. L. Grande, E. B. O. da Rosa, G. Schiwietz, and I. J. R. Baumvol, Appl. Phys. Lett. **92**, 164102 (2008).
[29] J. Lindhard, Nucl. Instrum. Methods **132**, 1 (1976).
[30] D. H. Jakubassa, J. Phys. C **10**, 4491 (1977).
[31] H. Wang, Y. Chen, Y. Kaneta, and S. Iwata, J. Phys.: Condens. Matter **18**, 10663 (2006).
[32] E. D. Palik and B. Ghosh (editors), *The Electronic Handbook of optical Constants of Solids* (Academic Press, San Diego, 1998).
[33] J. C. Moreno-Marín, I. Abril, S. Heredia-Avalos, and R. Garcia-Molina, Nucl. Instrum. Methods Phys. Res., Sect. B **249**, 29 (2006).
[34] H. Kreckel, S. Krohn, L. Lammich, M. Lange, J. Levin, M. Scheffel, D. Schwalm, J. Tennyson, Z. Vager, R. Wester, A. Wolf, and D. Zajfman, Phys. Rev. A **66**, 052509 (2002).
[35] G. L. Tan, M. F. Lemon, D. J. Jones, and R. H. French, Phys. Rev. B **72**, 205117 (2005).
[36] H. Jensen, Z. Phys. **77**, 722 (1932).
[37] D. Schmaus, F. Abel, M. Bruneaux, C. Cohen, A. L'Hoir, G. Della Mea, A. V. Drigo, S. Lo Russo, and G. G. Bentini, Phys. Rev. B **19**, 5581 (1979).
[38] G. Amsel, G. Battistig, and A. L'Hoir, Nucl. Instrum. Methods Phys. Res., Sect. B **201**, 325 (2003).
[39] D. Schmaus and A. L'Hoir, Nucl. Instrum. Methods Phys. Res., Sect. B **4**, 317 (1984).